nature communications

Article

https://doi.org/10.1038/s41467-025-59857-1

A ventral pallidum-locus coeruleus-lateral hypothalamus pathway modulates brain arousal in freely behaving and isoflurane-anesthetized male mice

Received: 8 November 2024

Accepted: 7 May 2025

Published online: 16 May 2025

Check for updates

Xiang-Ying Xu[1,2,3], Yue Xiao[1,4], Xu Liu[1], Yue Huang[1], Ying Ji[1], Yawei Ji[1], Yuan Gao[1], Su Liu[2,3,5], Jian-Jun Yang[6], Jun-Li Cao[1,2,3,5,7] ✉, Chunyi Zhou[1,2,3,7] ✉ & Cheng Xiao[1,2,3,7] ✉

Much progress has been made in the understanding of the neural circuits associated with sleep and anesthesia. As an important component among these circuits, the forebrain nuclei have been frequently interrogated. This study demonstrates that glutamatergic (Glu) neurons in the ventral pallidum (VP) enhance activity upon salient stimuli and state-dependently modulate brain arousal and motor activity in freely behaving male mice, and bidirectionally regulate the induction of and emergence from isoflurane general anesthesia. We delineate a neural pathway, consisting of VP Glu neurons→noradrenergic (NA) neurons in the locus coeruleus (LC)→the lateral hypothalamus (LH) in male mice, controlling the release of noradrenaline in the LH and state-dependently modulated brain arousal, motor activity, and isoflurane general anesthesia through α2a receptors in the LH. Therefore, the VP^{Glu}-LC^{NA}-LH pathway and α2a receptors in the LH may be promising state-dependent regulators of brain arousal in both freely behaving and anesthetized states.

Arousal is an important psychological process that requires specific adjustment for the proper functioning of various physiological activities[1]. During awake states, the level of arousal shows an inverted U-shaped relationship with the performance of attention, learning, and memory[2–4]. Accumulating studies have extensively examined the molecular, cellular, and neural circuit mechanisms involved in the transitions between wakefulness and sleep and made significant advances in understanding these physiological processes[5–8]. Disturbance or dysfunction of arousal-related neural circuits can impact the sleep-wakefulness cycle, resulting in conditions such as insomnia or excessive drowsiness. Furthermore, anesthesia, characterized by unconsciousness, shares certain physiological features and neural circuitry with sleep[9–12]. While much progress has been made in studying the neural circuits associated with sleep and anesthesia, the mechanisms regulating arousal levels in awake states have received less attention.

The basal forebrain plays an important role in regulating sleep-wakefulness and anesthesia. Specifically, GABAergic, glutamatergic (Glu), and cholinergic neurons within the basal forebrain modulate the sleep-wakefulness cycle[13,14]. Activation of these neurons promotes the

[1]Jiangsu Province Key Laboratory of Anesthesiology, School of Anesthesiology, Xuzhou Medical University, Xuzhou, Jiangsu, China. [2]Jiangsu Province Key Laboratory of Anesthesia and Analgesia Application Technology, Xuzhou Medical University, Xuzhou, Jiangsu, China. [3]NMPA Key Laboratory for Research and Evaluation of Narcotic and Psychotropic Drugs, School of Anesthesiology, Xuzhou Medical University, Xuzhou, Jiangsu, China. [4]Department of Anesthesiology, Affiliated Hospital of Nantong University, Nantong, Jiangsu, China. [5]Department of Anesthesia, Affiliated Hospital of Xuzhou Medical University, Xuzhou, Jiangsu, China. [6]Department of Anesthesiology and Perioperative Medicine, The First Affiliated Hospital of Nanjing Medical University, Nanjing, Jiangsu, China. [7]These authors jointly supervised this work: Jun-Li Cao, Chunyi Zhou, Cheng Xiao. ✉e-mail: Cao0310@aliyun.com; chunyi.zhou@xzhmu.edu.cn; xchengxj@xzhmu.edu.cn

transition from sleep to wakefulness[5,8,15]. Lesioning or inactivating the basal forebrain facilitates the induction of anesthesia and increases the depth of anesthesia[10,11], while stimulating the basal forebrain accelerates emergence from anesthesia[16,17]. Cell-specific studies reveal that cholinergic and parvalbumin- and somatostatin-containing GABAergic neurons in the basal forebrain modulate anesthesia[18–21]. The ventral pallidum (VP), adjacent to the horizontal branch of the diagonal band of Broca and the substantia innominata, contains cholinergic, GABAergic, and Glu neurons and have distinct synaptic inputs and outputs[13,22,23]. However, further investigations are needed to address whether individual neuron types in the VP regulate anesthesia and which neural circuits mediate the regulation.

Activation of VP GABAergic and Glu neurons reduces non-rapid eye movement sleep and promotes wakefulness[24,25]. Stimulation of VP Glu neurons triggers avoidance behavior in freely-moving mice[22,26,27]. Nevertheless, there remain uncertainties regarding whether and through which neural circuits VP Glu neurons modulate brain arousal in freely behaving and anesthetized states. VP Glu neurons project to several brain regions involved in arousal, such as the ventral tegmental area, lateral habenula, lateral hypothalamus (LH), dorsal raphe, and locus coeruleus (LC)[22,26,28,29]. A recent study has shown that VP Glu neurons promote wakefulness from sleep through their projections to the LH but induce depression-like behaviors via their projections to the lateral habenula[25]. Noradrenergic (NA) neurons in the LC have widespread innervation throughout the central nervous system, controlling cortical arousal and affecting induction of and emergence from isoflurane anesthesia[30–32]. It remains unclear whether VP Glu neurons directly innervate LC NA neurons and whether this projection plays a role in regulating brain arousal, motor activity, and anesthesia.

Here, we show that VP Glu neurons respond to the alteration of the level of brain arousal and regulate brain arousal, motor activity, and isoflurane general anesthesia; the $VP^{Glu} \rightarrow LC^{NA} \rightarrow LH$ pathway partially mimics the function of VP Glu neurons through activation of α2a adrenoceptors in the LH. These results advance the understanding of neural circuit basis of arousal promoting effects of the ventral pallidum and provide potential targets to regulate brain arousal in both freely behaving and anesthetized mice.

Results

VP Glu neurons regulate arousal in freely behaving mice

To understand whether VP Glu neurons change activity when brain arousal is elevated in freely behaving mice, we monitored the activity of VP Glu neurons with fiber photometry while the mice encountered several salient events, because responses to salient stimuli are accompanied by enhanced brain arousal[5,33,34]. To fulfill this goal, we injected AAV-EF1α-DIO-GCaMP6 or AAV-EF1α-DIO-eYFP into the VP in Vglut2-Cre mice to specifically transfect GCaMP6 or eYFP into VP Glu neurons (Supplementary Fig. 1a, b); two weeks later, we placed the mice in an open field arena and observed that GCaMP6 signal in the VP was enhanced when GCaMP6 mice were rearing (Supplementary Fig. 1c, g), exploring a novel object (Supplementary Fig. 1d, h), interacting with a cage mate (Supplementary Fig. 1e, i), and subjected to an air puff onto the snout (Supplementary Fig. 1f, j). As the eYFP signal in the VP did not change when eYFP mice were in the same situations as GCaMP6 mice (Supplementary Fig. 1k, l), these data indicate that VP Glu neurons increase activity in response to salient stimuli, similar to previous findings[35,36].

A recent study reports that in freely behaving mice, brain arousal varies with the levels of motor activity: locomotive movement (LM), non-locomotive movement (NM), and immobile state (IM)[37]. We next examined whether persistent activation of VP Glu neurons alters motor activity in mice. We injected AAV-EF1α-DIO-hM3Dq-mCherry or AAV-EF1α-DIO-eYFP into the VP of Vglut2-Cre mice to transfect hM3Dq into 79.73 ± 2.44% ($n = 5$ mice) of VP Glu neurons (87.66 ± 2.26% of hM3Dq neurons co-labeled with CaMKII) (Fig. 1a, b). This strategy allowed enhancing the activity of VP Glu neurons with clozapine-N-oxide (CNO, 3 μM) (Fig. 1c, d and Supplementary Fig. 2c, d). We observed that intraperitoneal injection of CNO (1 mg/kg) reduced time spent in IM ($t = 3.33$, $P = 0.02$), while increased time spent in LM ($t = 2.65$, $P = 0.04$), number of episodes of NM ($t = 5.68$, $P = 0.001$) and LM ($t = 5.12$, $P = 0.002$), and episode duration in NM ($t = 2.58$, $P = 0.04$) (Fig. 1e–h) (Two-tailed paired t-tests). We compared 60 min electroencephalograph (EEG) signal in mice recorded before and 30 min after CNO injection (Supplementary Fig. 2a). We observed that CNO activation of VP Glu neurons increased c-Fos-positive neurons in the VP (Supplementary Fig. 2c, d) and reduced the power of delta and theta waves, but increased the power of alpha and gamma waves (Supplementary Fig. 2e–g). Therefore, stimulation of VP Glu neurons elevates the level of motor activity and brain arousal in freely behaving mice.

To understand whether the baseline activity of VP Glu neurons is necessary to maintain normal motor activity, we injected AAV-EF1α-DIO-KORD-mCitrine or AAV-EF1α-DIO-eYFP into the VP of Vglut2-Cre mice to allow chemogenetic inhibition of firing in VP Glu neurons with salvinorin B (SALB) (Supplementary Fig. 3a–d). Subcutaneous administration of SALB (3 mg/kg) in KORD mice significantly prolonged time spent and number of episodes in IM, but not in other motor activity states (Supplementary Fig. 3e–h), increased the power of delta wave, but reduced the power of alpha and gamma waves in EEG (Supplementary Fig. 3i–k). These data suggest that inhibition of VP Glu neurons have sedative effect on freely behaving mice.

To explore whether stimulation of VP Glu neurons changes brain arousal in freely behaving mice during different motor activity states, we performed optogenetic stimulation of VP Glu neurons at a higher temporal resolution than chemogenetic technique and examined EEG in mice during various motor activity states (Fig. 1e). We injected AAV-EF1α-DIO-ChR2-eYFP or AAV-EF1α-DIO-eYFP into the VP in Vglut2-Cre mice to transfect ChR2 or eYFP into VP Glu neurons for blue light activation of these neurons (Fig. 1i–l). Consistent with a previous study[37], we observed that EEG spectra in freely behaving mice differ among different motor activity states: power of delta wave was significantly higher in IM than in NM and LM, whereas power of beta and gamma waves were significantly higher in NM and LM than in IM (Fig. 1m–r). We placed the mice in an open field arena, started EEG recording, visually identified their motor activity states, then delivered 1 min blue light stimulation (5 ms, 4 mW, 20 Hz) into the VP (Fig. 1e; Supplementary Fig. 2g). We observed that blue light stimulation of VP Glu neurons caused a rightward shift in spectrum of EEG signal with a peak at alpha band (Fig. 1m–r). As illustrated in Fig. 1s–u, blue light stimulation significantly reduced the power of delta ($t = 11.72$, $P < 0.0001$) and theta ($t = 7.02$, $P = 0.0004$) waves, but increased the power of alpha ($t = 7.09$, $P = 0.0002$), beta ($t = 2.73$, $P = 0.03$) and gamma ($t = 6.76$, $P = 0.0005$) waves in mice during IM; it decreased the power of delta (NM: $t = 4.37$, $P = 0.003$; LM: $t = 3.70$, $P = 0.008$) and theta (NM: $t = 7.01$, $P = 0.002$; LM: $t = 12.58$, $P < 0.0001$) waves, but increased the power of alpha (NM: $t = 5.73$, $P = 0.0007$; LM: $t = 4.29$, $P = 0.004$) and beta (NM: $t = 2.29$, $P = 0.06$; LM: $t = 4.15$, $P = 0.004$) waves during LM and NM (Two-tailed paired t-tests). As a reduction of the power of delta band was reported with enhancement in arousal[37], our data support the notion that stimulation of VP Glu neurons is sufficient to elevate arousal level in freely behaving mice, while its effect on gamma wave depends on the motor activity states of the mice.

VP Glu neurons alter isoflurane anesthesia induction and emergence

Our data show that VP Glu neurons modulate brain arousal and motor activity in freely behaving mice. Luo et al demonstrated that VP Glu neurons are implicated in sleep and wakefulness[25]. We wondered whether bilateral modulation of VP Glu neurons with optogenetic techniques regulates isoflurane general anesthesia. To implement

https://doi.org/10.1038/s41467-025-59857-1

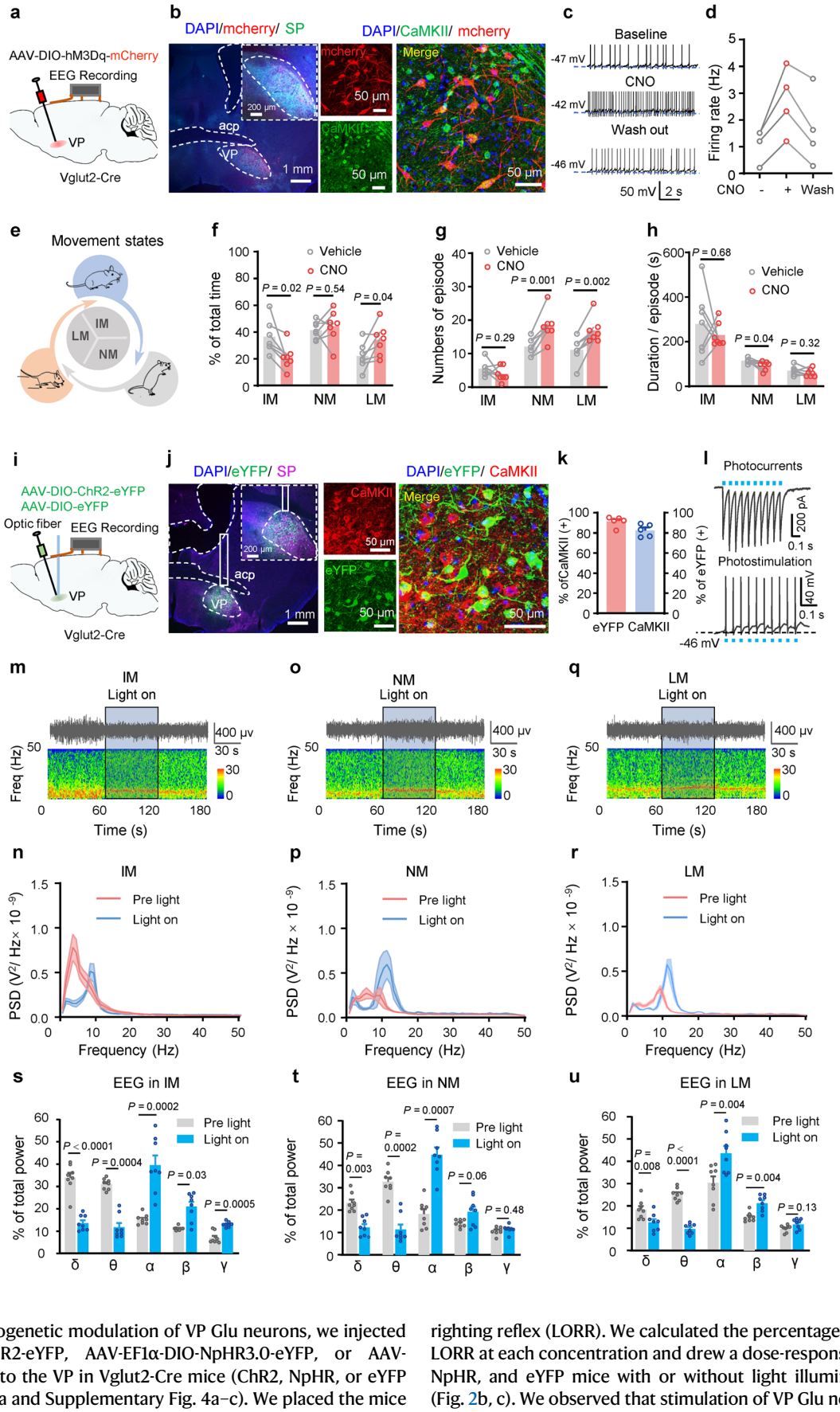

bidirectional optogenetic modulation of VP Glu neurons, we injected AAV-EF1α-DIO-ChR2-eYFP, AAV-EF1α-DIO-NpHR3.0-eYFP, or AAV-EF1α-DIO-eYFP into the VP in Vglut2-Cre mice (ChR2, NpHR, or eYFP mice) (Figs. 1i-l, 2a and Supplementary Fig. 4a–c). We placed the mice in an induction box equilibrated with 0.6-1.2% isoflurane by an increment of 0.1% and maintaining for 15 min at each concentration, and recorded the concentration of isoflurane the mice showed loss of righting reflex (LORR). We calculated the percentage of mice showing LORR at each concentration and drew a dose-response curve in ChR2, NpHR, and eYFP mice with or without light illumination in the VP (Fig. 2b, c). We observed that stimulation of VP Glu neurons induced a rightward shift in the dose-response curve for isoflurane-induced anesthesia in ChR2 mice (Fig. 2e); in contrast, inhibition of VP Glu neurons caused a leftward shift in the dose-response curve for

Fig. 1 | VP Glu neurons regulate movement and brain arousal in mice. **a** Schematic diagram and representative image showing virus injection into the VP (demarcated by substance P-antibody staining) (green) and EEG recording in Vglut2-Cre mice. **b** Verification of virus expression (red) in glutamatergic (Glu) neurons (green) in the VP. **c**, **d** Representative traces and summary of firing rates in hM3Dq-expressing VP Glu neurons in brain slices before, during, and after bath perfusion of 3 μM CNO. **e** Classification of movement states in mice: immobile state (IM); non-locomotion movement including grooming and postural adjustments (NM); locomotion (LM). **f** % time in each state between half and 1.5 h after vehicle or CNO injection. **g** Number of episodes in each state. **h** Duration of episodes in each state. **i** Schematic diagram and representative image showing viral injection (green) and optical fiber implantation into the VP (purple) and EEG recording in Vglut2-Cre mice. **j** Verification of virus expression (green) in VP Glu neurons (red). **k** The specificity of the viral vector for the labeling of Glu neurons. $n = 4$ mice. **l** Blue light induced inward photocurrents (upper trace) and time-locked firing (lower trace) in a ChR2-expressing VP neuron. **m**, **o**, **q** Representative EEG traces (upper) and corresponding power spectrum (lower) before, during, and after optical stimulation (light on) in ChR2 mice. **n**, **p**, **r** Power spectrum of each state before and during light stimulation. **s**–**u** The relative power (percent of total) of different frequency bands in IM, NM, and LM states. The data is presented as the mean ± SEM in (**f**–**h**, **k**, **s**–**u**). Two-tailed paired *t*-test for (**f**–**h**, **s**–**u**). *P*-values are two-sided. $n = 8$ mice in (**e**–**h**, **n**–**u**). Mean ± SEM in (**f**–**h**, **k**, **n**, **p**, **r**–**u**). The source data are in the Supplementary Dataset, Source Data.xlsx. Statistical results are in Supplementary Table 1.

isoflurane-induced anesthesia in NpHR mice (Fig. 2f). Neither blue light nor yellow light illumination of the VP in eYFP mice caused a significant shift in the dose-response curve (Fig. 2d, e). These results suggest that stimulation and inhibition of VP Glu neurons reduce and increase sensitivity to isoflurane in mice, respectively.

To quantify the alteration of LORR in mice by VP Glu neuron stimulation, we then exposed the mice to 1.4% isoflurane and measured LORR with or without optogenetic modulation of VP Glu neurons (Fig. 2f). We observed that blue light illumination of VP Glu neurons increased the latency to LORR in ChR2 mice ($t = 3.16$, $P = 0.007$) but not in eYFP mice ($t = 0.42$, $P = 0.69$), while yellow light illumination of VP Glu neurons shortened time to LORR in NpHR mice ($t = 2.42$, $P = 0.03$) but not in eYFP mice ($t = 0.57$, $P = 0.58$) (Fig. 2g, h). After 30 min maintenance of anesthesia with 1.4% isoflurane, we discontinued isoflurane administration, delivered only air into the induction chamber, and recorded latency until recovery of righting reflex (RORR) (a standard parameter for assessing anesthesia emergence) (Fig. 2f). Our data show that blue light illumination of the VP accelerated RORR in ChR2 mice ($t = 8.70$, $P < 0.0001$); in contrast, yellow light illumination of the VP postponed RORR in NpHR mice ($t = 3.93$, $P = 0.002$) (Fig. 2i, j). Neither blue nor yellow light illumination changed RORR in eYFP mice (blue light: $t = 0.59$ $P = 0.57$; yellow light: $t = 0.64$, $P = 0.53$) (Fig. 2i, j). We implemented the established methodology described by Taylor et al.[38] to quantitatively assess motor activity recovery in mice during anesthesia emergence (Fig. 2k). This quantitative assessment scale evaluates five distinct recovery parameters: limb movement, cephalic motion, vibrissae activity, righting reflex, and ambulatory capacity. Each parameter was graded on a 0 to 2 scale corresponding to absent, partial, or complete functional recovery. We found that optogenetic bidirectional modulation of VP Glu neurons differentially regulated anesthetic recovery kinetics: photostimulation significantly accelerated ($t = 6.81$, $P < 0.0001$) while photoinhibition markedly prolonged ($t = 5.39$, $P < 0.0001$) the restoration of motor function during anesthesia emergence (Fig. 2l–o).

These data suggest that VP Glu neurons modulate sensitivity to isoflurane and the temporal kinetics of both induction and emergence of isoflurane-induced general anesthesia. This establishes VP Glu neurons as a neural substrate governing consciousness state transitions during anesthetic challenges.

We next examined whether VP Glu neurons regulate brain arousal states during the maintenance of anesthesia. Burst suppression ratio (BSR) and spectrum of EEG are two sets of parameters for assessing the depth of anesthesia. In our experimental setting, after induction of anesthesia with 1.4% isoflurane, burst suppression occurred in all mice when anesthesia was maintained with 1.4% isoflurane, but disappeared in all mice when isoflurane concentration was adjusted to 0.8% or lower. Therefore, in the following experiments, we used 1.4% and 0.8% isoflurane to maintain anesthesia and assessed BSR and EEG spectrum, respectively (Fig. 3a–p). After 20 min maintenance of anesthesia with 1.4% isoflurane, we delivered 1 min blue light (20 Hz, 5 ms, 4 mW) into the VP in ChR2 and eYFP mice (Fig. 3a) and observed that it reversibly reduced BSR in ChR2 mice ($t = 7.70$, $P = 0.0008$), but not in eYFP mice ($t = 0.31$, $P = 0.99$) (Fig. 3b, c). In contrast, optogenetic inhibition of VP Glu neurons enhanced BSR in NpHR mice ($t = 6.36$, $P = 0.001$) (Fig. 3d–f). After 20 min maintenance of anesthesia with 0.8% isoflurane (Fig. 3g), optogenetic stimulation of VP Glu neurons (in ChR2 mice) attenuated the power of delta wave ($t = 2.95$, $P = 0.01$) and theta wave ($t = 2.61$, $P = 0.03$), but enhanced that of beta wave ($t = 5.14$, $P = 0.001$) (Fig. 3h–k). In contrast, optogenetic inhibition of VP Glu neurons (in NpHR mice) increased the power of delta wave ($t = 3.22$, $P = 0.01$), but reduced the power of beta ($t = 3.42$, $P = 0.008$) and gamma ($t = 3.02$, $P = 0.014$) waves (Fig. 3l–p).

In addition, we delivered 1 mW blue light (5 ms, 20 Hz) into ChR2 mice, and observed that it significantly accelerated recovery of motor function, slightly reduced BSR, but did not affect LORR, RORR, and EEG spectrum (Supplementary Fig. 5a–j). The effects of 1 mW blue light were significantly weaker than 4 mW blue light (Supplementary Fig. 5a–j).

These data suggest that VP Glu neurons regulate the brain arousal during anesthesia with different depths.

To understand whether the activity of VP Glu neurons differ with the depth of anesthesia, we injected AAV-EF1α-DIO-GCaMP6s or AAV-EF1α-DIO-eYFP into the VP, implanted an optical fiber into the VP of Vglut2-Cre mice and performed fiber photometry recording from VP Glu neurons when the mice were anesthetized with either 0.8% or 1.4% isoflurane (Supplementary Fig. 1a, b, S6a). We observed that anesthesia is accompanied with a reduction of GCaMP6 signal in GCaMP6 mice exposed to either 0.8% or 1.4% isoflurane, and the reduction was much stronger upon exposure to 1.4% isoflurane than to 0.8% isoflurane (Supplementary Fig. 6b, c). During emergence from anesthesia, the recovery of the GCaMP6 signal was much slower in 1.4% isoflurane than in 0.8% isoflurane (Supplementary Fig. 6d, e). Note that the reduction of GCaMP6 signal after initiation of isoflurane exposure and the recovery of GCaMP6 signal after discontinuation of isoflurane exposure occurred most dramatically after LORR and RORR, respectively, and the extent of the alterations were stronger when the mice were exposed to 1.4% isoflurane than when they were exposed to 0.8% isoflurane (Supplementary Fig. 6f, g). These data indicate that isoflurane reduces the activity of VP Glu neurons in a concentration- and time-dependent manner and induces anesthesia when the activity of VP Glu neurons reduced to a certain level. Therefore, the reduction of the activity of VP Glu neurons may represent the anesthetized states and the depth of anesthesia.

VP Glu neurons innervate locus coeruleus noradrenergic neurons

To address which downstream nuclei were subjected to significant excitation by photo-stimulation of VP Glu^{ChR2} neurons, we performed c-Fos-staining in brain sections from mice that received optogenetic stimulation of VP Glu neurons while they were awake and anesthetized (Supplementary Fig. 7a–c). We found that optogenetic stimulation of VP Glu neurons increased the number of c-Fos-positive neurons in the lateral habenula (LHb), ventral tegmental area (VTA), locus coeruleus (LC), ventrolateral periaqueductal gray (vlPAG), and lateral

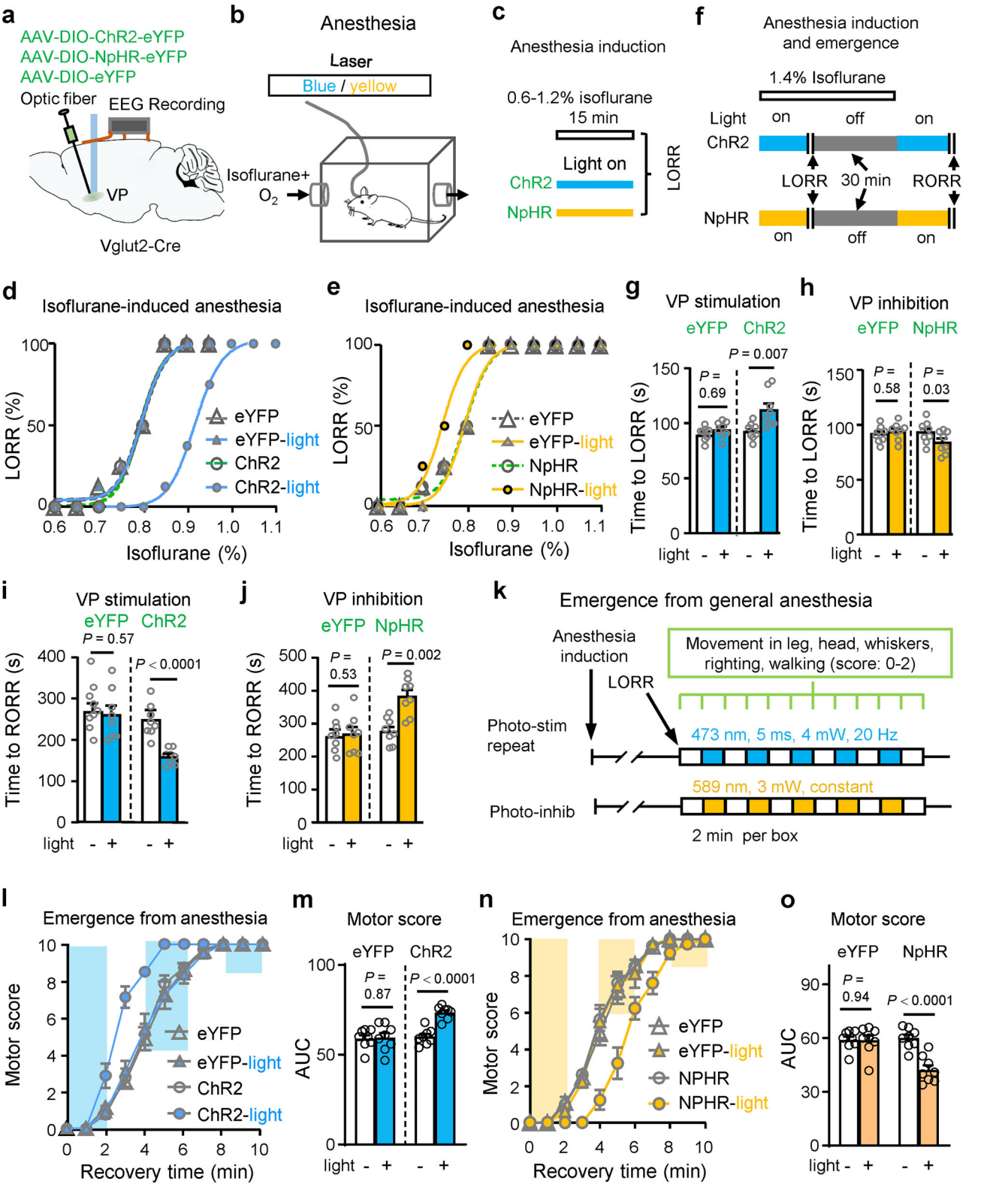

hypothalamus (LH) (Supplementary Fig. 7d–m). These nuclei are among the downstream nuclei of the VP, as reported in previous studies[22,26,39,40]. Therefore, these nuclei may be directly or indirectly involved in the modulation of brain arousal, motor activity, and anesthesia by VP Glu neurons.

VP Glu neurons have been reported to form monosynaptic connections with the LHb and VTA neurons, but cell-specific studies suggest that these two pathways may facilitate the induction of anesthesia[41,42], opposite from the effect of stimulation of VP Glu neurons on anesthesia (Figs. 2, 3). In contrast, many sophisticated studies have implicated LC noradrenergic (NA) neurons in arousal[43,44], and chemogenetic stimulation of LC NA neurons attenuates the power of delta wave in EEG and accelerates emergence from isoflurane general anesthesia[32]. These effects are similar to those of VP Glu neurons. Therefore, we performed the following experiments to address whether VP Glu neurons directly innervate LC NA neurons.

Fig. 2 | VP Glu neurons regulate isoflurane anesthesia induction and emergence. a Schematic diagram for virus injection into the VP and EEG recording in Vglut2-Cre mice. **b** Apparatus used for anesthesia with isoflurane in mice. **c** Time line for exposure to 0.6–1.2% (with 0.1% increment) isoflurane (15 min each concentration) until loss of righting reflex (LORR). **d** Time line for emergence from general anesthesia induced by 1.4% isoflurane and maintained by 1.4% isoflurane for 30 min. Emergence was assessed with recovery of righting reflex (RORR). **e** Dose–response curves (fitted) for isoflurane-induced LORR without (eYFP, ChR2) or with (eYFP-light, ChR2-light) blue light illumination in the VP of eYFP and ChR2 mice. **f** Dose–response curves (fitted) of isoflurane-induced LORR without (eYFP, NpHR) or with (eYFP-light, NpHR-light) yellow light illumination in the VP of eYFP and NpHR mice. **g**, **h** LORR time before and during blue and yellow light illumination in eYFP and ChR2, eYFP and NpHR mice, respectively. **i**, **j** Time to RORR before and during blue and yellow light illumination in eYFP and ChR2, eYFP and NpHR mice, respectively. **k** Motor scores after discontinuation of isoflurane. **l**, **m** Time courses and area under the curve (AUC) of the motor score recovery from isoflurane anesthesia in eYFP and ChR2 mice without (blank bars) or with blue light illumination (blue bars) in the VP. **n**, **o** Time courses and AUC of motor scores during recovery from isoflurane anesthesia in eYFP and NpHR mice without (blank bars) or with (yellow bars) yellow light illumination in the VP. Two-tailed paired *t* tests for (**g**–**j**, **m**, **o**). *P*-values are two-sided. $n = 8$ mice in each group. Mean ± SEM in (**g**–**j**, **l**–**o**). The source data are in the Supplementary Dataset, Source Data.xlsx. Statistical results are in Supplementary Table 1.

First, we injected AAV-EF1α-DIO-eYFP into the VP in Vglut2-Cre mice and observed eYFP-labeled fibers around LC NA neurons, containing tyrosine hydroxylase (TH, a rate-limiting enzyme for the synthesis of noradrenaline) (Fig. 4a, b). Second, we injected DBH (dopa-β-hydroxylase)-Cre mice with AAV-CaMKII-ChR2-eYFP into the VP to transfect ChR2 into VP Glu neurons and injected AAV-EF1α-DIO-mCherry into the LC to label LC NA neurons (Fig. 4c). Six weeks later, we performed ex vivo brain slice patch-clamp recordings from mCherry-labeled LC NA neurons and detected blue-light-evoked inward postsynaptic currents (photo-EPSCs) and spikes (Fig. 4d). Moreover, the photo-EPSCs were not completely blocked by the addition of TTX and 4-AP, but were eliminated by CNQX (Fig. 4e). We recorded photo-EPSCs in 77.8% (14/18) of NA neurons. Third, we used cell-type specific retrograde trans-synaptic rabies virus (RV) to probe the upstream neurons of LC NA neurons. We injected two helper viral vectors (AAV-EF1α-DIO-TVA-eGFP and AAV-EF1α-DIO-oRVG) into the LC and 21 days later, injected RV-CVS-EnvA(ΔG)-tdTomato into the LC in DBH-Cre mice (Fig. 4f, g). Ten days later, we detected tdTomato-labeled neurons in the VP at several coronal plains with a higher density around the bregma level (Fig. 4h and Supplementary Fig. 8a, b), and the great majority of tdTomato-labeled VP neurons were stained with the antibody of CaMKII, a marker protein for excitatory neurons (Fig. 4i, j). Thus, these data confirm that VP Glu neurons innervate LC NA neurons through monosynaptic connections and that these connections sufficiently modulate LC NA neurons.

To examine whether LC NA neurons innervated by VP Glu neurons respond to salient stimuli similarly to VP Glu neurons, we injected an anterograde trans-synaptic viral vector, AAV1/2-hSyn-DIO-Flp, into the VP and 2 weeks later we injected AAV-hSyn-fDIO-GCaMP6 into the LC in DBH-Cre mice (Fig. 4k). As VP Glu neurons were principal neurons in the VP that innervate LC NA neurons (Fig. 4i, j), the protocol allows transfecting GCaMP6 into LC NA neurons innervated by VP Glu neurons (Fig. 4l). Our immunofluorescent data confirmed that GCaMP6-transfected neurons were labeled by TH-antibody (Fig. 4l, m). We then performed fiber photometry from these neurons and observed that GCaMP6 signal in these LC NA neurons was enhanced when mice were rearing (Peak: $t = 6.04$, $P < 0.0001$; AUC: $t = 3.49$, $P = 0.002$), exploring a novel object (Peak: $t = 4.52$, $P = 0.0002$; AUC: $t = 4.13$, $P = 0.0005$), and interacting with a cage mate (Peak: $t = 5.13$, $P < 0.0001$; AUC: $t = 5.52$, $P < 0.0001$), but was reduced when mice received air puff onto the snout (Peak: $t = 4.84$, $P < 0.0001$; AUC: $t = 2.68$, $P = 0.014$) (Fig. 4n–t). Therefore, similar to VP Glu neurons, LC NA neurons innervated by VP Glu neurons respond to the enhancement of brain arousal upon salient stimuli. It should be noted that aversive stimulation increased the activity of VP Glu neurons, while decreased the activity of LC NA neurons receiving projection from VP Glu neurons. This paradoxical observation suggests that LC NA neurons may integrate strong inhibitory synaptic inputs mediating aversive responses, which functionally override the excitatory synaptic inputs from VP Glu neurons. Further investigations are needed to solve this issue.

We observed that in the process of isoflurane-induced anesthesia, GCaMP6 signal in LC NA neurons innervated by VP Glu neurons reduced after anesthesia induction and during anesthesia maintenance, but recovered after emergence from anesthesia, similar to that in VP Glu neurons (Supplementary Fig. 9a–f). These data support that LC NA neurons innervated by VP Glu neurons are modulated by isoflurane and are involved in anesthesia.

The VP^{Glu}– LC projection regulates arousal and anesthesia in mice

To address whether the VP^{Glu}-LC projection regulates brain arousal, we injected AAV-EF1α-DIO-ChR2-eYFP or AAV-EF1α-DIO-eYFP into the VP and implanted optical fiber into the LC in Vglut2-Cre mice (Fig. 5a–c). We delivered 1 min blue light (20 Hz, 5 ms, 4 mW) into the LC to stimulate the VP^{Glu}-LC projection, and found that it significantly changed EEG spectra when mice were in IM, NM, and LM (Fig. 5d–l), which are somewhat different from stimulation of VP Glu neurons (Fig. 1). Specifically, it reduced the power of delta wave when mice were in IM (δ: $t = 4.0$, $P = 0.005$) (Fig. 5d, e, g, h). In contrast, it increased the power of the delta wave ($t = 3.06$, $P = 0.02$), but reduced that of alpha wave ($t = 3.04$, $P = 0.02$) when the mice were in LM (Fig. 5f, i). In addition, it enhanced beta wave ($t = 2.50$, $P = 0.04$) and gamma wave ($t = 3.06$, $P = 0.02$) only in IM (Fig. 5j–l). These data indicate that stimulation of the VP^{Glu}-LC projection exerts a weaker effect on delta wave than that caused by stimulation of VP Glu neurons. During LM, multiple neural circuits may be recruited, and the regulation of the VP^{Glu}-LC^{NA} pathway may not provide a driving force as strong as stimulation of VP Glu neurons to further elevate arousal level. In contrast, stimulation of the VP^{Glu}-LC^{NA} pathway may counteract some neural circuits to reduce their effects on arousal. This may need further investigation to confirm. But this phenomenon clue that the VP^{Glu}-LC^{NA} pathway regulate brain arousal depending on motor activity states and may be a target to maintain arousal at a certain level.

We then applied bidirectional optogenetic modulation of the VP^{Glu}-LC projection to address whether it regulates anesthesia (Fig. 6a–d). We observed that stimulation of the VP^{Glu}-LC projection prolonged the latency to LORR in the presence of 1.4% isoflurane (eYFP: $t = 1.02$, $P = 0.35$, $n = 6$; ChR2: $t = 6.41$, $P = 0.001$, $n = 6$), but after 20 min anesthesia with 1.4% isoflurane, accelerated RORR (eYFP: $t = 0.32$, $P = 0.76$, $n = 6$; ChR2: $t = 2.94$, $P = 0.03$, $n = 6$.) and recovery of motor function (ChR2: $t = 11.55$, $P < 0.0001$, $n = 6$; eYFP: $t = 1.47$, $P = 0.20$, $n = 6$.) (Fig. 6e–i). On the contrary, after 20 min anesthesia with 1.4% isoflurane, optogenetic inhibition of the VP^{Glu}-LC projection accelerated LORR (eYFP: $t = 0.34$, $P = 0.75$, $n = 6$; NpHR: $t = 3.30$, $P = 0.02$, $n = 6$.), but postponed RORR (eYFP: $t = 0.32$, $P = 0.76$, $n = 6$; NpHR: $t = 2.62$, $P = 0.047$, $n = 6$.) and recovery of motor function (eYFP: $t = 1.47$, $P = 0.20$, $n = 6$; NpHR: $t = 5.33$, $P = 0.003$, $n = 6$.) (Fig. 6e, j–m). Unlike modulation of VP Glu neurons, modulation of the VP^{Glu}-LC projection did not alter BSR in anesthetized mice with 1.4% isoflurane (Blue light. eYFP: $t = 0.71$, $P = 0.51$; ChR2: $t = 0.79$, $P = 0.46$, $n = 6$ in each group) (Yellow light. eYFP: $t = 0.007$, $P = 0.99$; NpHR: $t = 0.37$, $P = 0.72$. $n = 6$ in each group) (Fig. 6n–q). Consistent with modulation of VP Glu neurons, optogenetic stimulation and inhibition of the VP^{Glu}-LC projection respectively reduced and enhanced EEG delta wave in ChR2 ($t = 4.63$, $P = 0.004$, $n = 6$) and NpHR mice ($t = 4.71$, $P = 0.005$, $n = 6$), respectively

https://doi.org/10.1038/s41467-025-59857-1

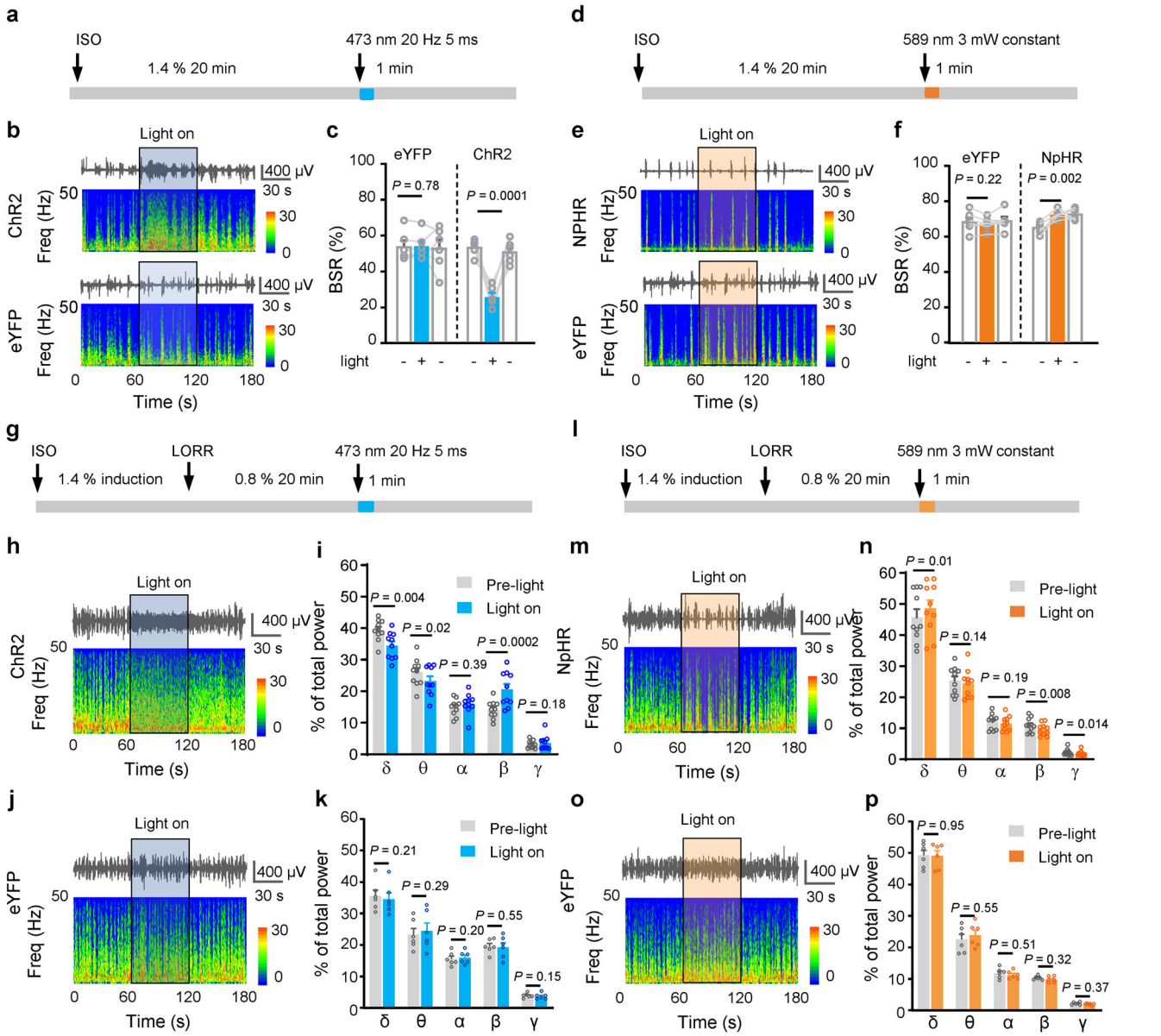

Fig. 3 | Effects of VP Glu neurons on EEG under isoflurane anesthesia. **a**, **d** Experimental protocol for examination of burst-suppression ratio (BSR) in the electroencephalograph (EEG) signal before and during optogenetic stimulation or inhibition of VP Glu neurons during anesthesia induced by 1.4 % isoflurane. The blue or yellow line represents the time window of light illumination of the VP. **b**, **c**, **e**, **f** Representative EEG traces, corresponding EEG power spectrum and summary of BSR before, during, and after blue or yellow light illumination in ChR2 / NpHR (upper) and eYFP mice (lower) under 1.4 % deep isoflurane anesthesia. $n = 6$ mice in each group. **g**, **l** Experimental protocol for examination of EEG spectrum during anesthesia with 0.8% isoflurane anesthesia. The blue or yellow line represents the time window of blue light (5 ms, 20 Hz, 4 mW) or yellow light (589 nm, constant, 3 mW) illumination. **h**–**k**, **m**–**p** Representative EEG traces, corresponding power spectra (lower), and summary of EEG waves under 0.8% isoflurane anesthesia in ChR2 ($n = 10$) / NpHR ($n = 10$) and eYFP ($n = 6$) mice before and during blue or yellow light illumination. One-way repeated measures ANOVAs in (**c**, **f**). Two-tailed paired t test for (**i**, **k**, **n**, **p**). P-values are two-sided. Mean ± SEM in (**c**, **f**, **i**, **k**, **n**, **p**). The source data are in the Supplementary Dataset, Source Data.xlsx. Statistical results are in Supplementary Table 1.

(Fig. 6r–u). These results indicate that the VP^{Glu}-LC projection partially mediates the role of VP Glu neurons in regulating brain arousal.

In this set of experiments, we applied the optogenetic technique to stimulate the terminals of VP Glu neurons in the LC. The caveat of this strategy is that action potentials in the terminals evoked by optogenetic stimuli may backpropagate to the somata and recruit downstream nuclei of activated VP Glu neurons other than the LC and confound the outcome. To mitigate this caveat, optogenetic stimulation of the VP^{Glu}-LC projection and chemogenetic inhibition of LC NA neurons innervated by VP^{Glu} neurons should be simultaneously performed to test the contribution of backpropagation of action potentials. For this purpose, we injected AAV1/2-hSyn-DIO-Flp and AAV-CaMKII-ChR2-eYFP into the VP of DBH-Cre mice; two weeks later, we injected AAV-hSyn-fDIO-hM4Di-mCherry and implanted optical fiber into the LC (Supplementary Fig. 10a, b). We observed that optogenetic stimulation of the VP^{Glu}-LC projection postponed the induction of anesthesia by 1.4% isoflurane and accelerated the emergence from anesthesia and the recovery of motor functions in mice (SupplementaryFig, S10c–g); during anesthesia with 0.8% isoflurane, stimulation of the VP^{Glu}-LC projection reduced the power of delta wave, but increased the power of alpha and beta waves (Supplementary Fig. 10h–j); these effects were blocked by chemogenetic

https://doi.org/10.1038/s41467-025-59857-1

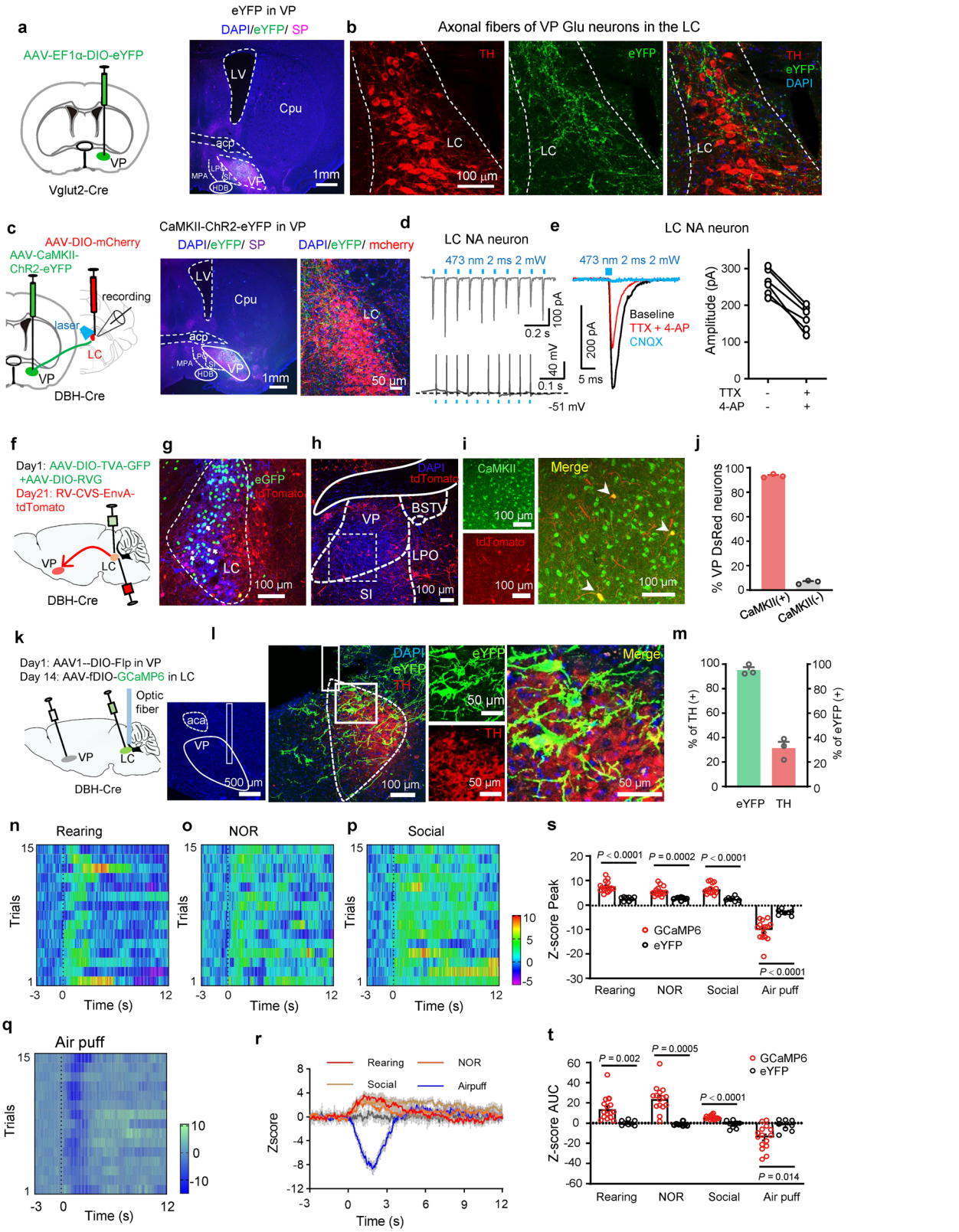

inhibition of LC NA neurons (Supplementary Fig. 10c–j). In freely behaving mice in IM and NM states, chemogenetic inhibition of LC NA neurons diminished the reduction in the power of the delta wave induced by stimulation of the VP^{Glu}-LC projection (Supplementary Fig. 10k, l). These data support that LC NA neurons play a significant role in modulatory effects of the VP^{Glu}-LC projection on both anesthesia and freely behaving states.

The VP^{Glu}– LC^{NA}–lateral hypothalamus pathway regulates arousal and anesthesia

We applied an anterograde trans-synaptic viral vector to probe the downstream targets of the VP^{Glu}-LC^{NA} projection. We injected AAV1/2-hSyn-DIO-Flp into the VP and 2 weeks later injected AAV-hSyn-fDIO-eYFP into the LC in DBH-Cre mice (Fig. 7a). The protocol allows transfecting eYFP into LC NA neurons innervated by VP Glu neurons

Fig. 4 | VP Glu neurons mono-synaptically innervate the locus coeruleus. **a** Schematic diagram for injection of AAV-EF1α-DIO-eYFP into the VP in Vglut2-Cre mice to label VP Glu neurons. **b** eYFP-labeled axonal fibers (green) of VP Glu neurons and noradrenergic (NA) neurons in the locus coeruleus (LC), labeled with tyrosine hydroxylase (TH)-antibody (red). **c** Diagram and typical images showing injection of AAV-CaMKII-ChR2-eYFP into the VP and AAV-EF1α-DIO-mCherry into the LC in DBH-Cre mice. **d** Blue light-evoked EPSCs at a holding potential of − 50 mV and spikes in an NA neuron (Vm = − 46 mV). **e** Representative traces and summary showing photo-EPSCs in LC NA neurons at baseline (black trace) and in the presence of 1 μM TTX + 100 μM 4-AP (red trace) or 20 μM CNQX (blue trace). $n = 6$ neurons. **f** Diagram of Cre-dependent retrograde tracing with rabies virus. **g** Example images of viral expression in the LC. Starter cells (white arrows) co-expressing AAV-DIO-TVA-eYFP (green) and RV-CVS-EnvA-ΔG-tdTomato (red). **h–j** Example images of tdTomato-labeled neurons in the VP Glu neurons. Most tdTomato (red) neurons were stained by CaMKII-antibody (green). $n = 3$ mice. **k** Schematic diagram of fiber photometry recording from LC NA neurons innervated by VP Glu neurons. **l**, **m** Example images and summary showing that most GCaMP6(+) LC neurons were stained by the TH-antibody. $n = 3$ mice. **n–t** Heat maps, averaged traces, peak z-score, and AUC of z-score of fluorescent signals in the VP of GCaMP6 and eYFP mice when the mice were rearing, recognizing novel object, encountering unfamiliar mice, and receiving an air puff. Two-tailed t tests for (**s**, **t**). GCaMP6: $n = 15$ trials from 5 GCaMP6 mice. eYFP: $n = 8$ trials from 4 eYFP mice. P-values are two-sided. Mean ± SEM in (**j**, **m**, **r–t**). The source data are in the Supplementary Dataset, Source Data.xlsx. Statistical results are in Supplementary Table 1.

(Fig. 7b, c). We detected eYFP-labeled axonal fibers in several nuclei, including the bed nucleus of the stria terminalis, lateral hypothalamus (LH), central amygdala, and subparafascicular nucleus of the thalamus (Fig. 7d). As the LH is an important nucleus regulating brain arousal and anesthesia[24,25,45], we postulated that the LH could be a valid downstream nuclei mediating the function of the VP^{Glu}-LC^{NA} projection. To prove this possibility, we injected AAV-hSyn-NE2M (a sensor of norepinephrine, NE) or AAV-hSyn-eYFP and implanted an optical fiber into the LH in mice (Supplementary Fig. 11a, b). Fiber photometry recording of NE2M signal in the LH showed that similar to the activity of VP Glu neurons, the release of NE in the LH was increased when the mice were exposed to salient stimuli: rearing, exploring novel object, interacting with a cage mate, and encountering an air puff (Supplementary Fig. 11c–l). These data suggest that similar to VP Glu neurons, NA terminals in the LH respond to elevation of brain arousal by salient stimuli.

To understand whether the VP^{Glu}-LC^{NA}-LH projection regulates the release of NE, we injected AAV1/2-hSyn-DIO-Flp and AAV-CaMKII-ChR2-eYFP into the VP of DBH-Cre mice; two weeks later, we injected AAV-hSyn-fDIO-hM4Di-mCherry into the LC and AAV-hSyn-NE2M into the LH and implanted optical fiber into the LC and LH (Fig. 7e, f). This set of experiments allows for the delivery of blue light into the LC to stimulate the VP^{Glu}-LC projection, fiber photometry recording of NE release in the LH, and chemogenetic inhibition of LC NA neurons innervated by VP Glu neurons. We observed that the stimulation of the VP^{Glu}-LC projection (5 ms light pulse, 20 Hz, 4 mW, 10 s) enhanced the release of NE, and the enhancement was dramatically attenuated when LC NA neurons were inhibited with chemogenetic technique (Peak: $t = 6.26$, $P < 0.001$; AUC: $t = 6.89$, $P < 0.001$,) (Fig. 7g–j). In freely behaving mice, NE2M signal increased when the mice were performing novel object recognition and social interaction, and were subjected to air puff onto the face (Supplementary Fig. 12a–f); but these increases were substantially attenuated after the mice received CNO injection to inhibit LC NA neurons innervated by VP Glu neurons (Supplementary Fig. 12a–g). In addition, in these mice, isoflurane anesthesia was accompanied by reduction of NE2M signal in the LH, which was significantly attenuated by chemogenetic inhibition of LC NA neurons (Supplementary Fig. 13a–f). These data support the notion that the VP^{Glu}-LC^{NA}-LH pathway controls the release of NE in the LH, which is inhibited during anesthesia.

According to the Allen Brain Atlas, α2a receptor is the most abundant adrenoceptor in the LH (Allen Institute for Brain Science, Experiment ID: 73615550). Using the patch-clamp technique, we proved that LH neurons were inhibited by guanfacine, an agonist of α2a receptor ($F_{(1.639,\ 19.66)} = 72.49$, $P < 0.0001$, $n = 13$) (Fig. 7k–n). To further support that the VP^{Glu}-LC^{NA}-LH projection regulates brain arousal through activating α2a receptors in the LH, we injected AAV1/2-hSyn-DIO-Flp into the VP, 2 weeks later, we injected AAV-hSyn-fDIO-hM3Dq-mCherry into the LC and implanted a cannula in the LH in DBH-Cre mice (Fig. 8a–c). This protocol allows for CNO-activation of NA terminals in the LH from LC NA neurons innervated by VP Glu neurons. We observed that administration of CNO (3 μM, 200 nl) into the LH reduced the duration of IM (% time: $t = 4.52$, $P = 0.008$) but increased the number of episodes in NM ($t = 7.67$, $P = 0.0004$) (Fig. 8d–f). These data suggest that stimulation of the VP^{Glu}-LC^{NA}-LH projection enhances motor activity in mice. When α2a receptors in the LH were blocked by yohimbine (10 μM, 200 nl), CNO-activation of LC^{NA} terminals in the LH no longer enhanced motor activity in mice (Fig. 8d–f). As illustrated in Fig. 8g–i, in freely behaving mice, CNO-activation of LC^{NA} terminals in the LH reduced the power of delta wave ($t = 3.97$, $P = 0.03$), but increased the power of gamma ($t = 4.06$, $P = 0.01$) wave; co-application of CNO and yohimbine into the LH did not change EEG spectrum. For 1.4% isoflurane-induced general anesthesia, CNO-activation of the VP^{Glu}-LC^{NA}-LH projection delayed LORR ($t = 3.75$, $P = 0.03$), shortened latency to RORR ($t = 3.48$, $P = 0.035$), and promoted recovery of motor function from anesthesia ($t = 13.78$, $P < 0.0001$); these effects were reversed by co-application of yohimbine with CNO into the LH (Fig. 8j–m). These data indicate that the VP^{Glu}-LC^{NA}-LH projection regulates motor activity and anesthesia, in which α2a receptors in the LH play an important role.

The VP^{Glu}– LH pathway regulates motor states but not anesthesia in mice

The VP^{Glu}-LH projection promotes transition from sleep to wakefulness[25]. But it has not been addressed whether this projection regulates anesthesia similar to the VP^{Glu}-LC^{NA} projection. To solve this puzzle, we injected AAV-EF1α-DIO-ChR2-eYFP into the VP of Vglut2-Cre mice, and implanted an optical fiber into the LH (Supplementary Fig. 14a, b). Using patch-clamp recording, we confirmed that in ChR2-expressing VP neurons, blue light evoked robust inward currents in the voltage-clamp mode and time-locked spikes in the current-clamp mode (Supplementary Fig. 14c); in LH neurons among eYFP-labeled fibers, blue light evoked an excitatory post-synaptic current, which is blocked by 1 μM TTX, but recovered after addition of 0.1 mM 4-AP (Supplementary Fig. 14d); 20 Hz blue light pulses were enough to enhance firing in LH neurons (Supplementary Fig. 14e, f). The mice were placed in an open field arena, and movement states were visually identified and light stimulation was delivered in each state. We observed that 20 Hz blue light stimulation of the VP^{Glu}-LH projection significantly reduced the power of delta wave in IM, but not in NM and LM (Supplementary Fig. 14h–p). These data suggest that the VP^{Glu}-LH projection promotes arousal, similar to the previous study[25].

We then examined the induction and emergence of anesthesia induced by 1.4% isoflurane (Supplementary Fig. 15a). As illustrated in Supplementary Fig. 15b–i, optogenetic stimulation of the VP^{Glu}-LH projection did not alter time to LORR and RORR, recovery of motor function after anesthesia, burst suppression ratio during anesthesia maintained by 1.4% isoflurane, and power of EEG waves during anesthesia maintained by 0.8% isoflurane.

https://doi.org/10.1038/s41467-025-59857-1

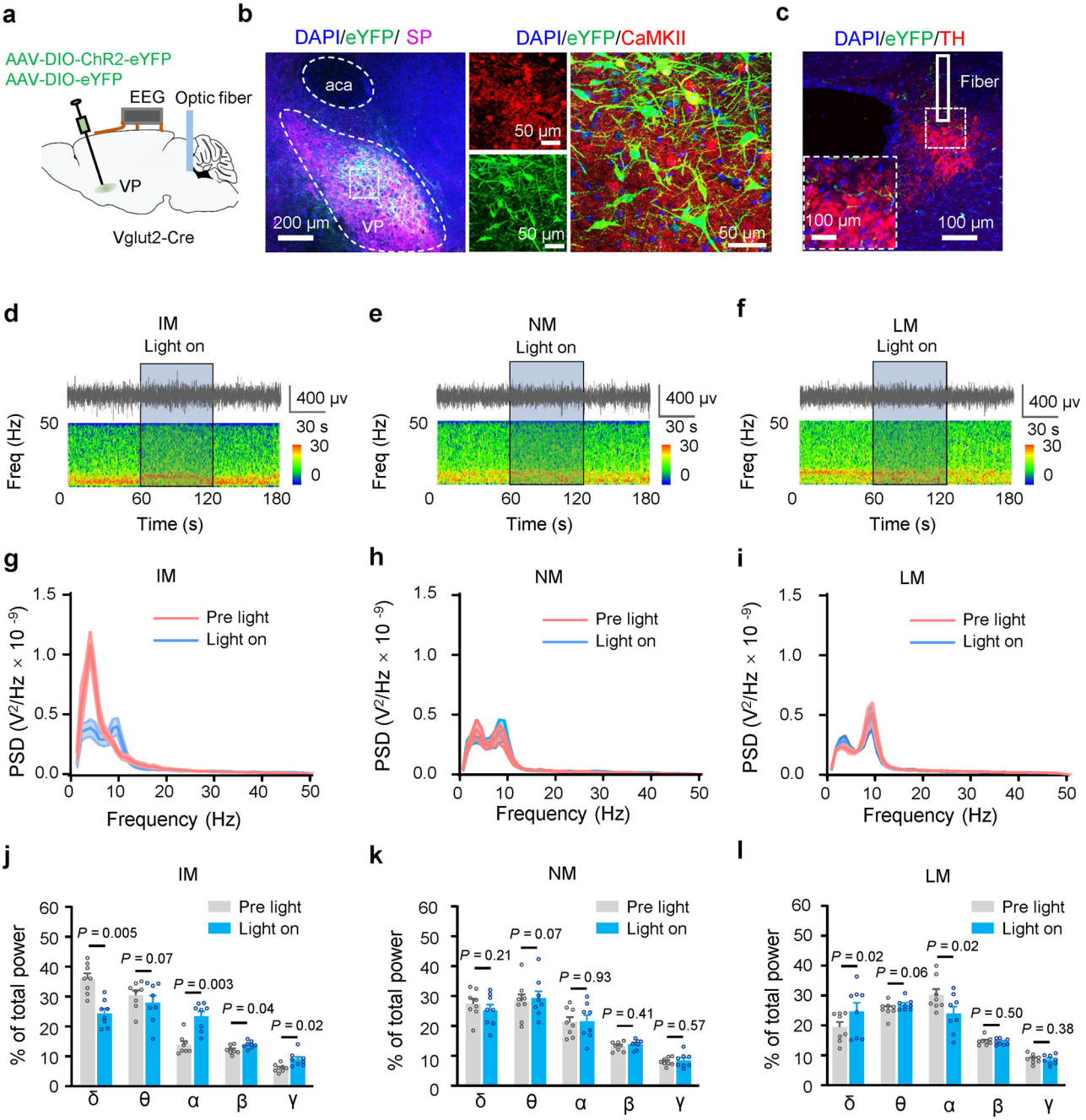

Fig. 5 | Activation of the VP-LC Glu projection enhances brain arousal at different movement states. a Schematic diagram of viral injection, optical fiber implantation, and EEG recording. **b** Verification of virus expression in VP Glu neurons. **c** An optical fiber was implanted in the LC. **d**–**f** Representative EEG traces (upper panel) and power spectra (lower) before, during, and after optical stimulation in ChR2 mice. (**g**–**i**) Power spectra before and during light stimulation in mice at different motor states. (**j**–**l**) % total power at EEG waves before and during light stimulation in mice at different motor states. Two-tailed paired *t* tests for (**j**–**l**). *P*-values are two-sided. Before vs during light illumination. $n = 8$ mice. Mean ± SEM in (**g**–**l**). The source data are in the Supplementary Dataset, Source Data.xlsx. Statistical results are in Supplementary Table 1.

Therefore, the VP^{Glu}-LH projection may not play a role in anesthesia similar to the VP^{Glu}-LC^{NA}-LH projection. To address whether these two projections are originated from different neuron populations, we injected retrograde viral vectors carrying either GFP or RFP into the LC or LH, and sacrificed the mice three weeks later (Supplementary Fig. 16a–c). We observed that few neurons were labeled by both GFP and RFP (Supplementary Fig. 16d, e). These data suggest that LC- and LH-projecting VP neurons may be separate neuron populations.

Therefore, LH-projecting VP Glu neurons may play a similar role to LC-projecting VP Glu neurons in regulating arousal in freely behaving mice but not in anesthetized mice.

Discussion

Accumulating evidence demonstrates that VP Glu neurons are implicated in a variety of behaviors. Electrophysiological and fiber photometry recordings from VP Glu neurons show that these neurons respond with increased activity not only to aversive stimuli but also to rewarding and novel stimuli[35,36], indicating that these neurons are critical in the processing of salience. The present study shows similar phenomena that VP Glu neurons enhanced activity when mice were exposed to salient stimuli. Neuromodulation studies show that stimulation of these neurons leads to avoidance behaviors[26,40], disrupts reward or drug seeking behavior[26,27], and interferes with motivation

https://doi.org/10.1038/s41467-025-59857-1

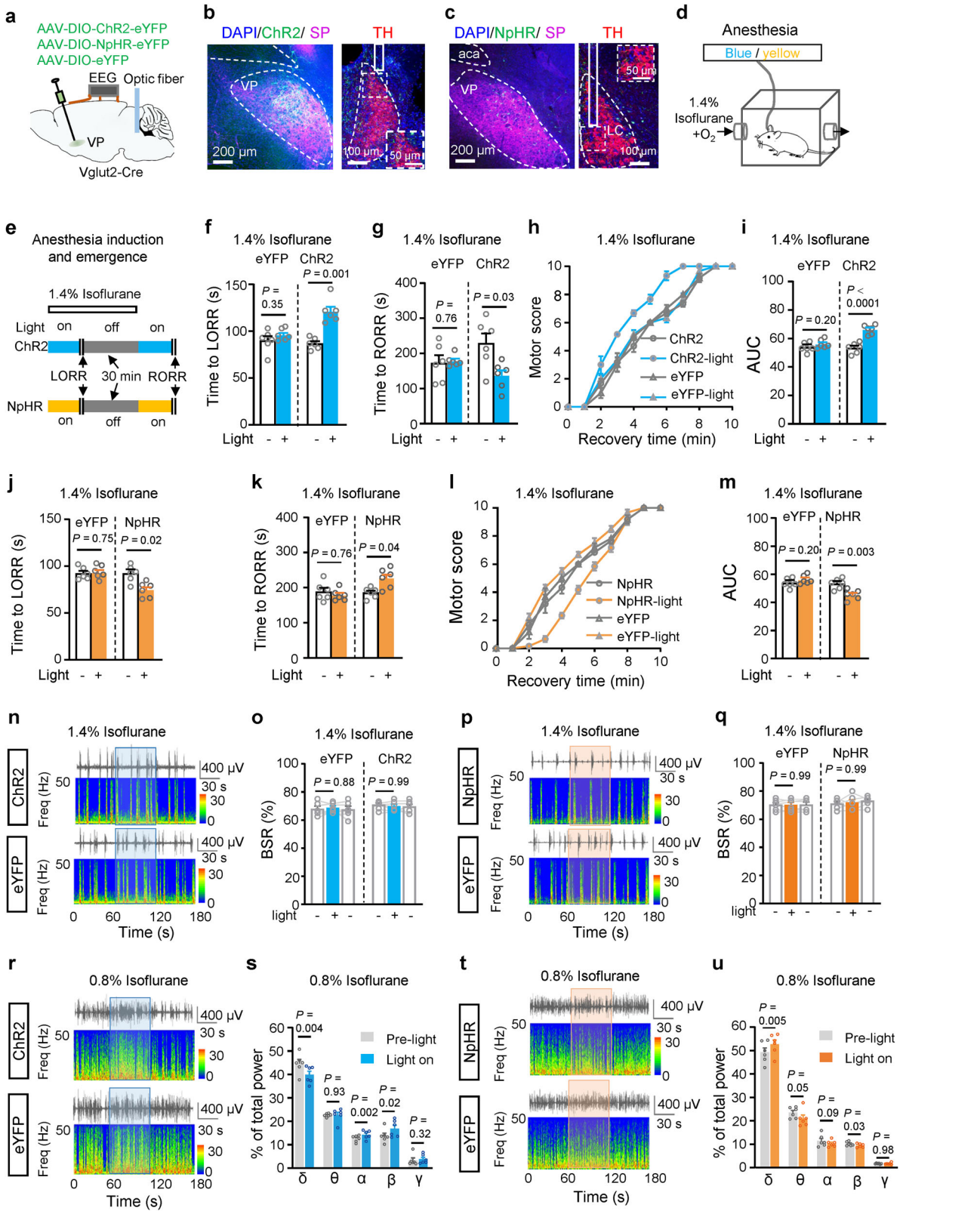

processing[46]. Therefore, VP Glu neurons are potential targets for the intervention of drug abuse and the treatment of psychiatric disorders. A recent study demonstrated that VP Glu neurons promoted transition from sleep to wakefulness and caused depression-like behavior, respectively, through their projections to the lateral hypothalamus and lateral habenula in mice[25]. In the present study, we reported that VP Glu neurons state-dependently regulated brain arousal and motor activity in freely behaving mice and altered the processes of general anesthesia. This study extends the scope of the physiological function of VP Glu neurons.

Using the fiber photometry technique, we observed that the activity of VP Glu neurons was enhanced by salient stimuli in freely behaving mice and reduced in anesthetized mice to an extent related to the depth of anesthesia. Our neuromodulation data suggest that VP

Fig. 6 | Regulation of LC NA neurons innervated by VP Glu neurons affects anesthesia in mice. a Schematic diagram of virus injection, optical fiber implantation, and EEG recording. **b**, **c** Representative images of ChR2- or NpHR-labeled VP Glu neurons and their terminals in the LC. An optical fiber was implanted in the LC. **d** Apparatus for isoflurane anesthesia. **e** Time line for examining general anesthesia induction and 30 min maintenance with 1.4% isoflurane and emergence from anesthesia. Blue light: 5 ms, 4 mW, 20 Hz, 2 min with 2 min intervals. Yellow light: constant, 3 mW, 2 min with 2 min intervals. **f**, **g** Time to LORR and RORR in eYFP and ChR2 mice with (blue) or without (blank) blue light illumination in the LC. **h**, **i** Motor function recovery without and with blue light illumination in the LC in eYFP and ChR2 mice. **j**, **k** Time to LORR and RORR in eYFP and NpHR mice with (yellow bars) or without (blank bars) yellow light stimulation in the LC. **l**, **m** Motor function recovery without and with yellow light illumination in the LC in eYFP and NpHR mice. **n**–**q** Representative EEG traces, corresponding power spectrum, and burst suppression ratio (BSR) in mice anesthetized with 1.4% isoflurane with and without blue or yellow light illumination in the LC. **r**–**u** Representative EEG traces, corresponding power spectrum, and summary of % power of EEG signal in mice anesthetized with 0.8% isoflurane with and without blue or yellow light illumination in the LC in ChR2 and NpHR mice. Two-tailed paired *t* tests for (**f**, **g**, **i**, **j**, **k**, **m**, **s**, **u**). One-way repeated measures ANOVAs in (**o**, **q**). *P*-values are two-sided. $n = 6$ mice in each group. Mean ± SEM in (**f**–**m**, **o**, **q**, **s**, **u**). The source data are in the Supplementary Dataset, Source Data.xlsx. Statistical results are in Supplementary Table 1.

Glu neurons regulate brain arousal, motor activity, and anesthesia. In freely behaving mice, chemogenetic stimulation of VP Glu neurons changed motor activity (with a reduction in immobile time, but an increase in LM time) and brain arousal (reduction in the power of delta waves, but increase in that of alpha and gamma waves); chemogenetic inhibition of VP Glu neurons increased immobile time and enhanced delta wave in EEG; optogenetic stimulation of VP Glu neurons at a higher temporal resolution reduced the power of delta wave, but increased the power of alpha and beta waves in all motor activity states, without altering the power of theta and gamma waves in IM and LM. These data suggest that VP Glu neurons promote brain arousal and motor activity in freely behaving mice, and its effects on brain arousal depend on movement states. In anesthetized mice, bidirectional modulation of VP Glu neurons regulated sensitivity to isoflurane, the induction of and emergence from isoflurane general anesthesia, and recovery of motor function, accompanied by alterations in EEG (burst suppression ratio and the power spectrum). Therefore, VP Glu neurons responded to salience and anesthesia and state-dependently regulated brain arousal in freely behaving and anesthetized mice.

Previous anatomical and neuromodulation studies have shown that stimulation of VP Glu neurons excites LHb neurons and then rostromedial tegmental area neurons, and subsequently activates VTA GABAergic neurons[26,27,39]. The consequence of excitation of either LHb Glu neurons or VTA GABAergic neurons is to inhibit arousal and facilitate anesthesia[41,47,48]. Therefore, these well-studied pathways may not mediate the effects of VP Glu neurons on arousal and anesthesia. Concerning the downstream pathways through which VP Glu neurons modulate anesthesia, we identified LC NA neurons as their monosynaptic targets and demonstrated that Glu neurons accounted for the great majority of VP neurons innervating LC NA neurons. Previous studies have demonstrated that the projections from LC NA neurons to the basal forebrain are among critical components in arousal-promoting circuits[5,32,43,44], and regulate anesthesia[32,49]. We observed that in freely behaving mice, stimulation of the VP^{Glu}-LC projection altered EEG spectrum depending on motor activity, meanwhile, the power of delta wave was reduced in IM and NM, but increased in LM. Bidirectional modulation of this projection regulated the induction of and emergence from isoflurane general anesthesia, but its effect on brain arousal depended on the depth of anesthesia (altered the power of delta wave when the mice were exposed to 0.8% isoflurane, but did not change burst suppression ratio when the mice were exposed to 1.4% isoflurane). Combining chemogenetic and optogenetic techniques, we demonstrated that LC NA neurons were important downstream neurons mediating arousal-promoting effect of VP Glu neurons by the VP^{Glu}-LC projection. We admit that the arousal-promoting effects of the VP^{Glu}-LC projection were not as strong as those of VP Glu neurons, suggesting that the LC is only one of the downstream nuclei of arousal-promoting VP Glu neurons and partially mediates the effects of VP Glu neurons. This hypothesis is supported by a recent study showing that the projection from VP Glu neurons to the LH enhances wakefulness[25].

The LH is an important nucleus to regulate brain arousal and anesthesia[24,25,45]. Neuroanatomical and electrophysiological evidence shows that both VP GABAergic and Glu neurons innervate the LH[24,25]. Using transsynaptic tracing and a cell-specific strategy, we revealed that the LH was also indirectly innervated by VP Glu neurons via LC NA neurons. Specifically, stimulation of the VP^{Glu}-LC pathway evoked the release of NE in the LH, which was significantly attenuated by inhibition of LC NA neurons innervated by VP Glu neurons. Furthermore, stimulation of the VP^{Glu}-LC^{NA} pathway to the LH altered motor activity and anesthesia probably through activating α2 adrenoceptors. Similarly, activation of α2 adrenoceptors in the ventrolateral preoptic nucleus reduced the depressant effects of isoflurane[50]. In contrast, systemic administration of dexmedetomidine, an α2 adrenoceptor agonist, induces loss of consciousness, enhances delta wave, and enhances the depth of sevoflurane general anesthesia[51,52]. This effect may result from inhibition of LC NA neurons by α2 adrenoceptor activation, followed by the reduction in the release of NE in the brain[53]. In the present study, we used a cell- and projection-specific strategy and local neuropharmacological intervention to stimulate the VP^{Glu}-LC^{NA}-LH pathway and in this process, α2 adrenoceptors in the LH were activated or blocked, and may regulate brain arousal different from systemic administration of dexmedetomidine.

Interestingly, our retrograde tracing data show that LC- and LH-projecting VP neurons were largely separated. Combining our behavioral experiments, we postulate that LC- and LH-projecting neurons both regulate natural arousal, while the former, but not the latter, mediates anesthesia regulation by VP Glu neurons. This highlights the important role of the NA pathway in these processes.

This study has at least four limitations. First, we defined movement states by offline analysis of video files according to stringent criteria. It is manual and cannot provide information about the transitions between different motor activities and brain arousal levels. Second, we did not record the electromyograph (EMG) signal. In this experimental configuration, we could not define whether in IM, mice are sleeping or not, as evidenced by our EMG recording (Supplementary Fig. 17). A Combination of EEG and EMG is able to provide physiological bases to rationally define motor states. Third, it has not been explained why individual components of the VP^{Glu}-LC^{NA}-LH pathway regulate brain arousal, movement states, and anesthesia in unidentical patterns. We observed that stimulation of VP^{Glu} neurons, the VP^{Glu}-LC projection, and the VP^{Glu}-LC^{NA}-LH projection regulated EEG spectrum, motor states, and anesthesia with different strengths. In addition, VP Glu neurons, LC NA neurons, and LH NA terminals responded in distinct patterns to salient stimuli. These may be explained by the complexity of axonal arborization and synaptic integration of these components. Fourth, among heterogenous neuron types in the LH[45], those expressing α2A adrenoceptors may play an important role in mediating arousal-promoting effects of the VP^{Glu}-LC^{NA}-LH pathway. Further investigations are need to address these puzzles.

In summary, our data advance the understanding of the role of VP Glu neurons in the regulation of brain arousal in awake and anesthetized mice. We delineated a tertiary pathway: VP^{Glu} neurons→LC^{NA} neurons→LH neurons that partially mediates the the effects of VP Glu neurons. α2 adrenoceptor in the LH may be an important target to modulate this pathway.

https://doi.org/10.1038/s41467-025-59857-1

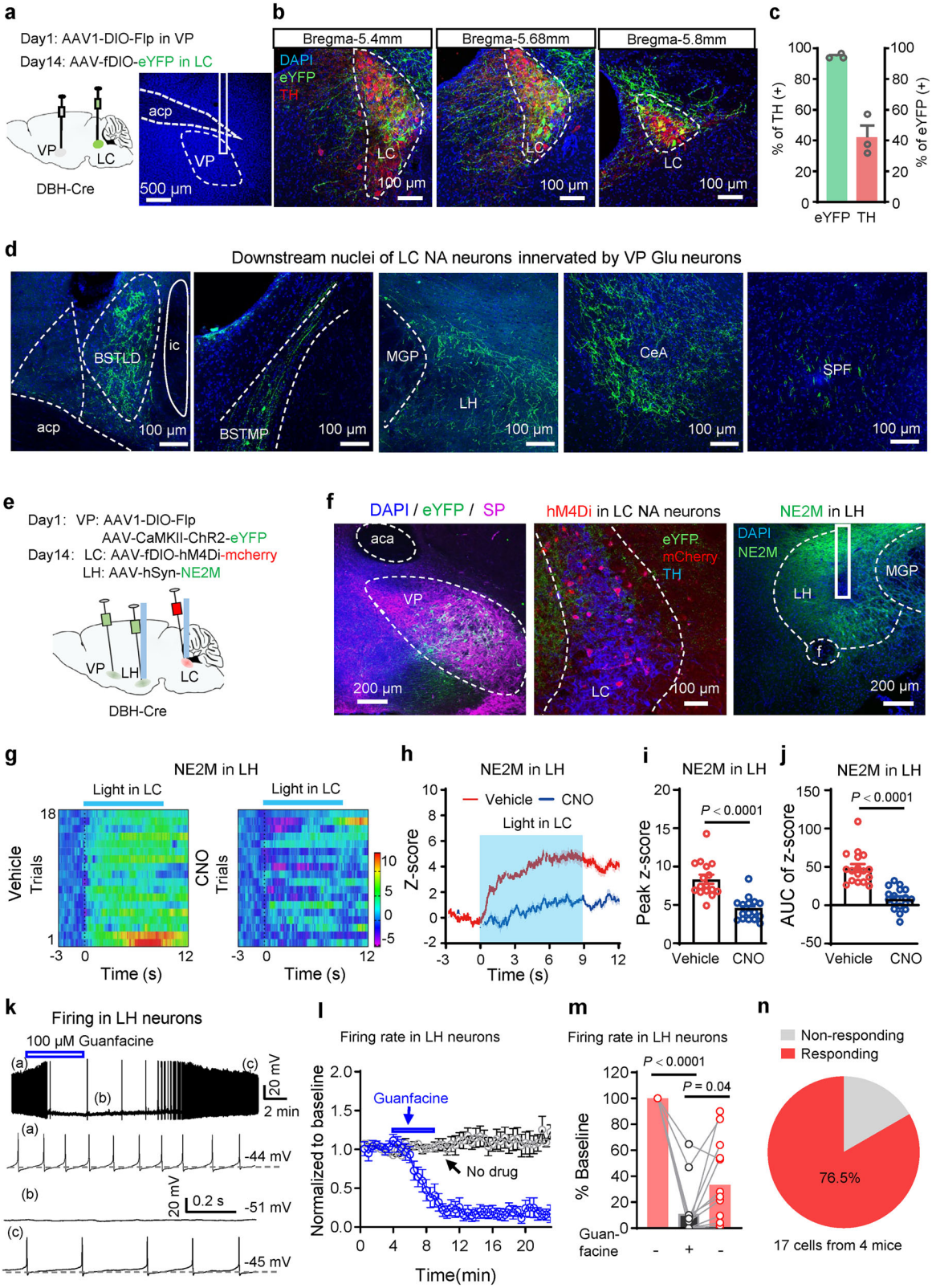

Methods

Ethics Statement

The care and use of animals and the experimental protocols (No. 202207S122) were approved by the Institutional Animal Care and Use Committee and the Office of Laboratory Animal Resources of Xuzhou Medical University.

Animals

Male C57BL/6 mice (6–8 weeks old) were purchased from the animal facility at Xuzhou Medical University. Male Vglut2-Cre (Stock No: 016963, Slc17a6$^{tm2(cre)Lowl}$/J) and DBH-Cre mice (Stock No. 033951, B6.Cg-Dbh$^{tm3.2(cre)Pjen}$/J) were purchased from Jackson Laboratory and bred in the animal facility at Xuzhou Medical University. The mice were

Fig. 7 | LC NA neurons innervated by VP Glu neurons project to the lateral hypothalamus. a Schematic diagram of virus injection. Anterograde trans-synaptic tracer AAV1-EF1α-DIO-Flp was injected into the VP in DBH-Cre mice. Two weeks later, AAV-hSyn-fDIO-eYFP was injected into the LC to label LC NA neurons innervated by VP glutaminergic neurons. **b**, **c** Representative images and summary of eYFP-labeled neurons stained with TH-antibody in the LC. $n = 3$ mice. **d** Representative images showing that downstream nuclei of LC NA neurons innervated by VP Glu neurons include the dorsal part and the medial posterolateral part of the bed nucleus of stria terminalis (BNST), the lateral hypothalamus (LH), the central amygdala (CeA), and the subthalamic parafascicular nucleus (SPF). **e** Schematic diagram of virus injection and optical fiber implantation. **f** Representative images of virus expression in the VP, LC, and LH, and locations of optical fibers in the LC and LH. **g**–**j** Heat map, averaged traces, peak, and area under curve (AUC) of peak of fluorescent signal in the LH of NE2M mice in response to optogenetic stimulation of the VP-LC Glu projection by i.p. injection of normal saline or CNO. $n = 18$ trials from 5 NE2M mice. **k**–**m** Representative traces, time course (blue, Guanfacine perfusion, n = 13; black, no drug application, $n = 8$, from 3 mice), and summary of firing in LH neurons before, during, and after bath perfusion of 100 μM guanfacine, an α2a receptor agonist. **n** A Pie chart showing the percentage of LH neurons inhibited by guanfacine. Two-tailed paired *t* tests in (**i**, **j**). One-way repeated measures ANOVA in (**m**). *P*-values are two-sided. Mean ± SEM in (**c**, **i**, **j**, **l**). Mean in histogram in (**m**). The source data are in the Supplementary Dataset, Source Data.xlsx. Statistical results are in Supplementary Table 1.

group-housed (≤ 4 per cage) in the animal facility with stable temperature (21–23 °C) and humidity (40%–70%). The 12-h light-dark cycle was programmed with lights turning on at 7:00 AM and turning off at 7:00 PM. Food and water were provided *ad libitum* to the mice. After 2–4 weeks' adjustment to their environment, the mice were randomly allocated into the groups described in the following experiments. Efforts were made to minimize animal suffering and to reduce the number of animals used.

Adenovirus associated viral (AAV) vectors

Brain VTA (Wuhan, China) provided the viral vectors: AAV-EF1α-DIO-GCaMP6f (Cat No. PT-0106), AAV-EF1α-DIO-hChR2(H134R)-eYFP(Cat No. PT-0001), AAV-EF1α-DIO-NpHR3.0-YFP (Cat No. PT-0006), AAV-EF1α-DIO-hM3Dq-mCherry (Cat No. PT-0042), AAV-EF1α-DIO-eYFP (Cat No. PT-0012), AAV-EF1α-DIO-mCherry (Cat No. PT-0013), AAV-CaMKII-ChR2-eYFP (Cat No. PT-0296), AAV-hSyn-fDIO-hM4Di-mCherry (Cat No. PT-0170), AAV-hSyn-fDIO-GCaMP6s (Cat No. PT-0342), AAV-EF1α-DIO-TVA (Cat No. PT-0165), AAV-EF1α-DIO-RVG-eGFP (Cat No. PT-0061), and RV-CVS-ΔG-tdTomato (Cat No. R05002). Brain Case (Shenzhen, China) provided the viral vectors: AAV-EF1α-DIO-eGFP (Cat No. BC-0015), AAV-EF1α-DIO-KORD-mCitrine (Cat No. BC-0230), AAV-CaMKII-eYFP (Cat No. BC-0029), AAV1-hSyn-DIO-Flp (Cat No. BC-0178), AAV-hSyn-fDIO-eYFP (Cat No. BC-0241), AAV-hSyn-fDIO-hM3Dq-mCherry (Cat No. BC-0495), AAV-hSyn-NE2m (Cat No. BC-0267). AAV/Retro-hsyn-GFP (Cat No. AV200007-AV2retro) and AAV/Retro-hsyn-RFP (Cat No. AV200039-AV2 retro) were purchased from WZ Biosciences Inc. (Jinan, China). The titter of AAV (serotype 2/9 and serotype 1) is 1×10^{12} to 5×10^{12} vg/ml, and that of RV is 1×10^{8} to 5×10^{8} vg/ml.

Surgical procedures

Mice (3–4 months old, 25–30 g) were anesthetized with isoflurane (3% for induction, 1.4% for maintenance) and stabilized in a stereotaxic frame (RWD Life Sciences, Shenzhen, Guangdong, China). Mice were subjected to bilateral intracranial viral injection into the VP (150 nl) (Coordinates: AP, + 0.38 mm; ML, 1.30 mm; DV, − 5.1 mm) or into the LC (120 nl) (AP: − 5.6 mm; ML: 0.9 mm; DV: − 3.8 mm) or into the LH (200 nl) (AP: − 1.05 mm; ML: 1.1 mm; DV: 5.1 mm). Optical fibers were implanted in or above the VP [AP, + 0.38 mm; ML, 1.30 mm; DV, − 5.1 mm (for fiber photometry) or −4.9 mm (for optogenetic modulation)], LC [(AP: − 5.6 mm; ML: 0.9 mm; DV: − 3.8 mm for fiber photometry or − 3.6 mm for optogenetic modulation), and LH (AP: − 1.05 mm; ML: 1.1 mm; DV: 5.1 mm). The mice were allowed to recover for 2 − 4 weeks before behavioral tests, optogenetic manipulation, electrophysiological recording, and morphological assay.

For local drug application into the LH (AP: − 1.05 mm; ML: 1.6 mm; DV: 4.65 mm), a stainless-steel guide cannula (26 G) (RWD Life Science, Shenzhen, China) was implanted at an angle of 6 degree and the tip of the cannula was 500 μm above the viral injection site in the LH (AP: − 1.05 mm; ML: 1.6 mm; DV: 4.65 mm) as the needle (30 G) for drug delivery is 500 μm longer than the cannula. 200 nl CNO (3 μM) and Yohimbine (10 μM) was delivered with a 10 μl Hamilton syringe at a speed of 50 nl per min controlled by a Micro4 WPI microinjection pump (Lubbock, TX, USA).

Meloxicam (4 mg/kg) was subcutaneously administered once per day for 3 days' postoperative pain relief.

Fiber photometry

To monitor the activity of VP and LC neurons and the release of noradrenaline in the LH, a fiber photometry instrument (ThinkerTech, Nanjing, Jiangsu, China)[54–57] was used. To quantify the activity changes, we averaged 3 s GCaMP6 signal (F) just before the response to give a mean (Mean) and standard deviation (SD) and transformed the data into z-scores [(F-Mean)/SD]. The peak response was quantified by the peak z-scores or the area under the response curve.

Motor activity assessment

Mice were acclimatized in the testing room for at least 1 h, then, were individually placed in an open field arena (a transparent plexiglass cylinder, 30 cm in diameter and 40 cm in height). The behaviors of the mice were recorded with a camera on the side of the cylinder. The data recorded between the 10th and 20th minutes in the arena were visually analyzed offline. The motor states of the mice were classified into three categories: (a) immobile state (IM); (b) non-locomotive movement (NM), when the mouse remained in the same spot moving four limbs, head, or trunk; (c) locomotion (LM), when the mouse roamed in the arena. For optogenetic manipulation, we started light stimulation after mice remained in a state for at least 10 s, and included data for analysis when mice remained in the same state throughout light stimulation.

Electrophysiological recordings

EEG and EMG recordings. EEG and EMG recordings were performed as described in a previous report[58]. The mice were anesthetized with isoflurane (3% for induction and 1.5% for maintenance of anesthesia) and stabilized in a stereotactic frame. An incision was made along the midline of the skin on the skull, and three holes were drilled on the skull: one above the frontal lobe (for the first EEG channel; AP + 2.0 mm, ML + 0.7 mm), one above the central lobe (for the second EEG channel; AP: − 1.3 mm, ML + 1.3 mm), and one above the lateral parietal lobe (for the reference and ground; AP − 3.5 mm, ML − 2.5 mm). Stainless steel screws soldered to electrode leads (softened stainless-steel wire) were twisted into the craniotomy holes. The electrode leads were connected to a headmount that fits to the headstage of a Plexon DigiAmp16 (16 channels) amplifier (Hong Kong, China) or a 4-channel PowerLab amplifier (AD Instruments, Dunedin, New Zealand). The headmount, electrode leads, and screws were fixed to the skull with dental cement. One softened 0.1 mm thick stainless-steel wire was soldered on the headmount, and the other end was inserted into the trapezius muscles. Finally, the incision was closed. The EEG and EMG signals were analyzed with NeuroExplorer 5.0 (Plexon, Hong Kong, China) or LabChart (AD Instruments, Dunedin, New Zealand).

https://doi.org/10.1038/s41467-025-59857-1

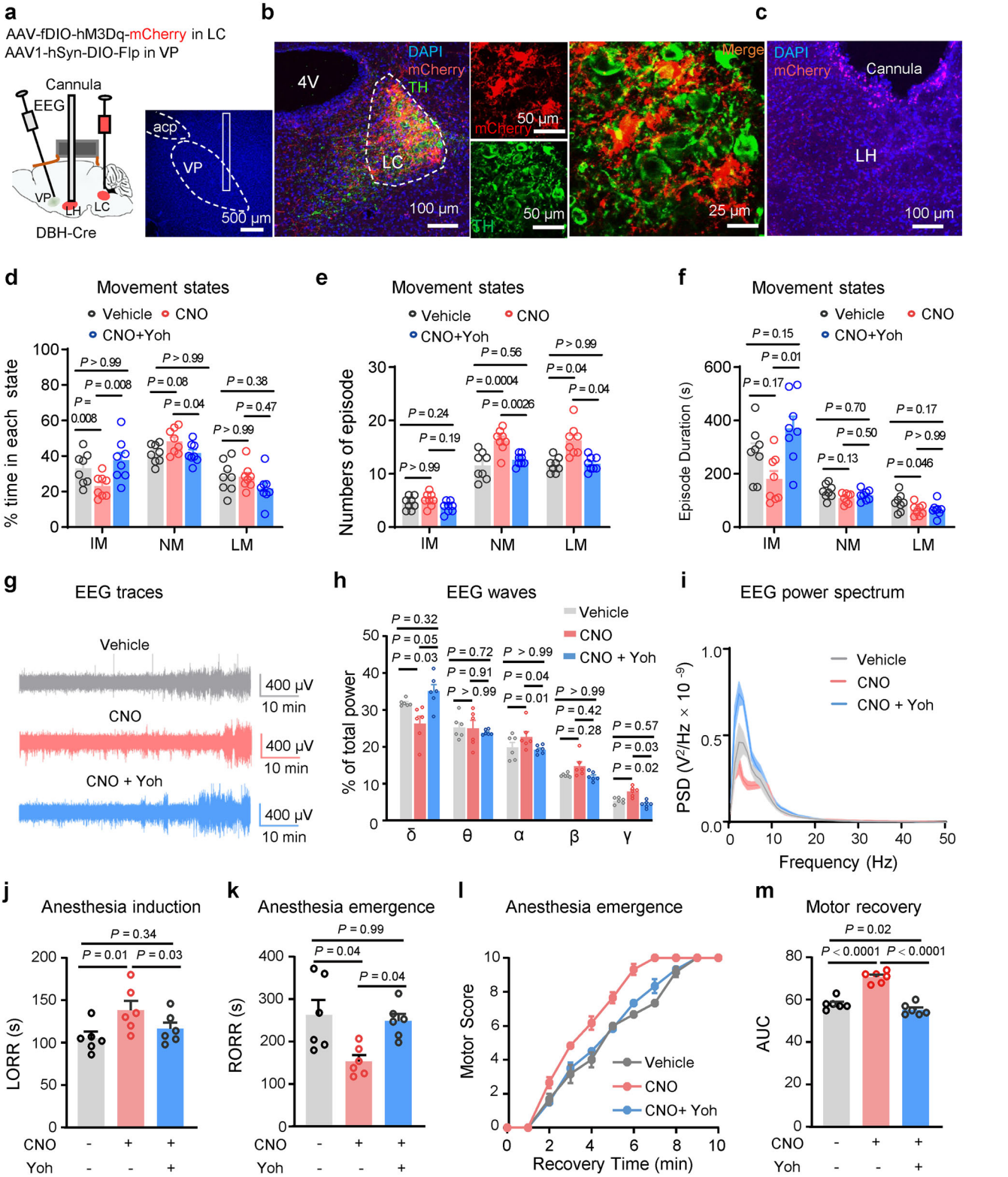

Fig. 8 | The VP^{Glu}-LC^{NE}-LH pathway regulates arousal and anesthesia through α2a receptor in the LH. a Schematic diagram of virus injection, cannula implantation, and EEG recording in DBH-Cre mice. **b**, **c** Images showing virus expression in the LC and a cannula in the LH. **d**–**f** % time, number of episodes, and total duration in each motor state between 1 to 1.5 h after Vehicle, CNO and CNO + Yohembine (Yoh) injection. **g**–**i** Representative traces of EEG signals, % power of EEG waves, and EEG power spectrum between 0.5 and 1.5 h after injection of vehicle, CNO, or CNO +Yoh into the LH, in freely behaving mice. **j**–**m** Time to LORR in 1.4% isoflurane and RORR and motor score recovery after 20 min anesthesia with 1.4% isoflurane after delivery of Vehicle, CNO and CNO+Yoh into the LH. One-way repeated measures ANOVAs in (**d**–**f**, **h**, **j**, **k**, **m**). *P*-values are two-sided. $n = 6$ in each group. Mean ± SEM in (**d**–**f**, **h**–**m**). The source data are in the Supplementary Dataset, Source Data.xlsx. Statistical results are in Supplementary Table 1.

Patch-clamp recordings. Brain slices were prepared according to a modified version of a protocol described previously[57,59]. In brief, the mice were deeply euthanized with CO_2 and then decapitated. The brain was removed and cut into 300-μm-thick parasagittal (for recording of LC NA neurons) or coronal (for recording of VP and LH neurons) slices with a vibratome (VT-1200S, Leica, Nussloch, Germany) while immersed in ice-cold modified sucrose-based artificial cerebral spinal fluid (sACSF), containing (in mM) 85 NaCl, 75 sucrose, 2.5 KCl, 1.25 NaH_2PO_4, 4.0 $MgCl_2$, 0.5 $CaCl_2$, 24 $NaHCO_3$, and 25 glucose. The sACSF was constantly bubbled and saturated with 95% O_2 / 5% CO_2 (carbogen). Brain slices containing the VP or LC or LH were allowed to recover at 32 ± 1 °C in carbogenated sACSF for 1 h, and then were transferred into carbogenated normal ACSF, containing (mM) 125 NaCl, 2.5 KCl, 1.2 NaH_2PO_4, 1.2 $MgCl_2$, 2.4 $CaCl_2$, 26 $NaHCO_3$, and 11 glucose, saturated with 95% O_2 / 5% CO_2 (carbogen) and maintained at room temperature. Individual slices were transferred to the recording chamber and superfused (1.5–2.0 ml/min) with carbogenated ACSF at 32 ± 0.5 °C.

Neurons in brain slices were visualized with a Nikon FN-1 upright microscope (Tokyo, Japan) equipped with a CCD-camera (Flash 4.0 LTE, Hamamatsu, Hamamatsu City, Japan) and near-infrared and fluorescent (green and red) illumination. Electrophysiological signals were recorded at a sampling rate of 10 kHz with a patch-clamp system, consisting of a MultiClamp 700B amplifiers, a Digidata 1550B analog-to-digital converters, and the MultiClamp Commander 2.0 and Clampex 10.7 softwares (Molecular Devices, San Jose, CA, USA), installed in a computer. The patch electrodes were pulled with a P-1000 pipette puller (Sutter Instrument, Novato, CA, USA) and had a resistance of 4–6 MΩ when filled with an intrapipette solution containing (in mM) 135 K gluconate, 5 KCl, 0.2 EGTA, 0.5 $CaCl_2$, 10 HEPES, 2 Mg-ATP, and 0.1 GTP, pH: 7.2, osmolarity around 300 mOsm. The junction potential between the patch pipette and the bath solution was nulled just before gigaseal formation. The data were discarded if the series resistance (11–20 MΩ) changed by > 20% during whole-cell recordings.

An optical fiber (200 μm in diameter, NA 0.37) was positioned 200 μm away from the patch-clamped neurons in the VP and LC to deliver blue light (460 nm, 5 ms, 2 mW) to stimulate ChR2-labeled neurons and axons and lime light (550 nm, 1 s, 2 mW) to inhibit NpHR-labeled neurons[57,59]. A PlexBright 4-channel light source (Plexon Inc., Hong Kong, China) was used to deliver blue light and lime light.

Anesthesia

For isoflurane anesthesia, we used an induction box with an inlet connected to an isoflurane evaporator (RWD Life Science Co. Ltd, Shenzhen, Guangdong, China) and an outlet connected to a gas indicator (FI-21) (Riken Keiki, Tokyo, Japan) to measure the concentration of isoflurane. The concentration-response relationship between isoflurane and anesthesia was examined with a previously published protocol[60]. We placed a mouse into the induction box and ventilated a mixture of air and increasing concentrations of isoflurane, commencing at 0.6% with an increment of 0.1% at 15-min intervals. Before transition to the next concentration, righting reflex was examined by rolling the induction box to let the mouse lay on its back. The conscious mouse has the ability to right itself and stands on feet within seconds. The loss of righting ability refers to the loss of the righting reflex (LORR). The concentration of isoflurane produced LORR was recorded as the effective anesthetic threshold. We calculated the percentage of mice showing LORR at each concentration and drew a concentration-response curve, which was fitted with a nonlinear regression model (GraphPad Prism software). After termination of isoflurane exposure, motor function of the mice was scored every two minutes until the recovery of righting reflex (RORR)[38]. RORR refers to the restoration of the ability for a mouse to right itself after being placed on its back. The motor function of mice during emergence from anesthesia was evaluated based on movements in the legs, head, and whiskers, as well as righting and ambulatory behaviors. Each item was scored on a scale from 0 to 2, where 0 indicates no activity, 1 indicates weak activity, and 2 indicates normal activity.

Immunofluorescence assay

After being sacrificed with CO_2, mice were immediately subjected to cardiac perfusion with phosphate buffer saline (PBS), followed by 4% paraformaldehyde (PFA) in PBS. Brains were removed, post-fixed in PFA for 12 h in 4 °C refrigerator, and dipped in 30% sucrose at 4 °C for 2–3 days until sank. 30 μm thick brain sections were prepared with a CM1950 Leica cryostat (Nussloch, Germany) and mounted onto clean glass slides. Immunostaining and microscopy were performed according to a standard protocol[57,59].

For immunostaining, brain sections were sequentially washed in PBS for 10 min, blocked in 5% donkey serum (Jackson ImmunoResearch, Code: 017-000-121, RRID: AB_2337258) for 1 h and 0.1% Triton X-100 in PBS for 90 min, and incubated with primary antibodies in 1% donkey serum and 0.1% Triton X-100 in PBS at 4 °C for 24–48 h.

Primary antibodies include (1) rabbit anti-c-Fos IgG, 1:2000, c-Fos (9F6) Rabbit mAb, Cell Signaling Technology, Cat No. 2250 S; (2) Chicken anti-TH, Aves Lab, 1:500, Cat No.TYH; (3) Rabbit anti-CaMKII, 1:400, ABclonal, Cat No. A22611; (4) Rat anti-Substance P, 1:100, Sigma-Aldrich, Cat No. MAB356.

The sections were immersed into fresh PBS three times (10 min each), and incubated with secondary antibodies for 90 min at room temperature.

Secondary antibodies, provided by Jackson ImmunoResearch Laboratories, Inc. (West Grove, PA, USA), include (1) Donkey anti-rabbit Alexa 488, 1:500, Code: 711-545-152, RRID: AB_2313584; (2) Donkey anti-rabbit Alexa Cy3, 1:500, Code: 711-165-152, RRID: AB_2307443; (3) Donkey anti-rabbit Alexa 647, 1:500, Code: 711-605-152, RRID: AB_2492288; (4) Donkey anti-chicken Alexa Cy3, 1:500, Code: 703-165-155, RRID: AB_2340363; (5) Donkey anti-chicken Alexa 647, 1:500, Code: 703-605-155, RRID: AB_2340379; (6) Donkey anti-rat Alexa 647, 1:500, Code: 712-605-150, RRID: AB_2340693.

The sections were washed three times (10 min each) in PBS, dried in the dark, and then cover-slipped in antifade mounting medium (MeilunBio, Dalian, China) (Cat No. MA0222).

The antibody-stained brain sections were imaged under 10 × (NA, 0.45) and 20 × (NA, 0.80) Plan-Apochromat objectives equipped on an Olympus Fv-1000 confocal microscope (Olympus, Tokyo, Japan). The images were processed in Image J (NIH, Bethesda, MD, USA)[61].

Chemicals

4-aminopyridine (Cat No. HY-B0604), clozapine-N-oxide (CNO) (Cat No. HY-17366), CNQX disodium (FG9065) (Cat No. HY-15066A), Guanfacine (Cat No. HY-17416A), and yohimbine (Cat No. HY-N0127) were purchased from MedChem Express (Monmouth Junction, NJ, USA). SalvinorinB (Item No: 23582, CAS:92545-30-7) was purchased from Cayman Chemical Company (Ann Arbor, MI, USA). Tetrodotoxin (Cat No. 1078/1) was purchased from Tocris (Bristol, UK). Aladdin Scientific (Shanghai, China) provided meloxicam (Cat No. M129228).

Statistical analysis

For each experiment, we did an initial test with a sample size of 5 or 6, calculated the variation (standard deviation) in the parameters, and used the power analysis function in SigmaPlot 14.0 software ($\alpha = 0.05$, $\beta = 0.85$) to estimate the minimal samples needed to obtain reliable statistics. Sample sizes are all greater than these values.

For optogenetic and behavioral experiments, mice were randomly assigned to experimental groups. All summarized data are expressed as the mean ± SEM. The error bars in histograms, time courses, and input-output curves are SEM. Two-tailed paired or unpaired *t*-tests, one-way ANOVAs followed by post-hoc Bonferroni or Tukey tests, and one-way repeated-measures ANOVAs with post-hoc Bonferroni tests and Geisser-Greenhouse correction were used to compare the

behavioral and electrophysiological data, as indicated in the figure legends. If data did not pass equal-variance and / or normal distribution evaluation, they were compared with the Mann-Whitney rank sum test or by one-way ANOVA rank tests. Source data in all figures are provided in a Supplementary Data file (Source Data.xlsx). In all tests, a value of two-sided $P < 0.05$ was considered statistically significant. GraphPad Prism (version 8.0) was used for all statistical analyses. All statistics in the main figures were listed in the Results section and Supplementary Table 1, and those in Supplementary Figs. were reported in the corresponding figure legends and Supplementary Table 2.

When we finished each experiment, we sacrificed every mouse for histological evidence to confirm the expression of viral vectors and localization of optical fiber for optogenetic modulation and fiber photometry recording, and cannula for intracranial drug delivery. The images in Figures are representative ones from mice we collected data in individual experiments.

Reporting summary

Further information on research design is available in the Nature Portfolio Reporting Summary linked to this article.

Data availability

Source data are provided in this paper.

Code availability

This study uses commercially available software for data acquisition and analysis, and does not generate new codes.

References

1. Berridge, C. W. Noradrenergic modulation of arousal. *Brain Res. Rev.* **58**, 1–17 (2008).
2. Alhola, P. & Polo-Kantola, P. Sleep deprivation: Impact on cognitive performance. *Neuropsychiatr. Dis. Treat.* **3**, 553–567 (2007).
3. McCoy, J. G. & Strecker, R. E. The cognitive cost of sleep lost. *Neurobiol. Learn Mem.* **96**, 564–582 (2011).
4. Van Dongen, H. P., Maislin, G., Mullington, J. M. & Dinges, D. F. The cumulative cost of additional wakefulness: dose-response effects on neurobehavioral functions and sleep physiology from chronic sleep restriction and total sleep deprivation. *Sleep* **26**, 117–126 (2003).
5. Liu, D. & Dan, Y. A motor theory of sleep-wake control: arousal-action circuit. *Annu. Rev. Neurosci.* **42**, 27–46 (2019).
6. Peng, W. et al. Regulation of sleep homeostasis mediator adenosine by basal forebrain glutamatergic neurons. *Science* **369**, eabb0556 (2020).
7. Scammell, T. E., Arrigoni, E. & Lipton, J. O. Neural circuitry of wakefulness and sleep. *Neuron* **93**, 747–765 (2017).
8. Xu, M. et al. Basal forebrain circuit for sleep-wake control. *Nat. Neurosci.* **18**, 1641–1647 (2015).
9. Brown, E. N., Purdon, P. L. & Van Dort, C. J. General anesthesia and altered states of arousal: a systems neuroscience analysis. *Annu Rev. Neurosci.* **34**, 601–628 (2011).
10. Colon, E. et al. Anesthesia, brain changes, and behavior: insights from neural systems biology. *Prog. Neurobiol.* **153**, 121–160 (2017).
11. Leung, L. S., Luo, T., Ma, J. & Herrick, I. Brain areas that influence general anesthesia. *Prog. Neurobiol.* **122**, 24–44 (2014).
12. Yang, Q., Zhou, F., Li, A. & Dong, H. Neural substrates for the regulation of sleep and general anesthesia. *Curr. Neuropharmacol.* **20**, 72–84 (2022).
13. Tingley, D., Alexander, A. S., Quinn, L. K., Chiba, A. A. & Nitz, D. A. Cell assemblies of the basal forebrain. *J. Neurosci.* **35**, 2992–3000 (2015).
14. Sharma, R., Sahota, P. & Thakkar, M. M. Chronic alcohol exposure reduces acetylated histones in the sleep-wake regulatory brain regions to ca use insomnia during withdrawal. *Neuropharmacology* **180**, 108332 (2020).
15. Pinto, L. et al. Fast modulation of visual perception by basal forebrain cholinergic neurons. *Nat. Neurosci.* **16**, 1857–1863 (2013).
16. Luo, T. & Leung, L. S. Basal forebrain histaminergic transmission modulates electroencephalographic activity and emergence f rom isoflurane anesthesia. *Anesthesiology* **111**, 725–733 (2009).
17. Dong, H. L., Fukuda, S., Murata, E., Zhu, Z. & Higuchi, T. Orexins increase cortical acetylcholine release and electroencephalographic activation through orexin -1 receptor in the rat basal forebrain during isoflurane anesthesia. *Anesthesiology* **104**, 1023–1032 (2006).
18. Cai, P. et al. Facilitation of behavioral and cortical emergence from isoflurane anesthesia by GABAergic neurons in basal forebrain. *J. Neurosci.* **43**, 2907–2920 (2023).
19. Cai, S. et al. Effect of basal forebrain somatostatin and parvalbumin neurons in propofol and isoflurane anesthesia. *CNS Neurosci. Ther.* **27**, 792–804 (2021).
20. Luo, T. Y. et al. Basal forebrain cholinergic activity modulates isoflurane and propofol anesthesia. *Front. Neurosci.* **14**, 559077 (2020).
21. Peng, Y. T., Yuan, C. D. & Zhang, Y. The role of the basal forebrain in general anesthesia. *Ibrain* **9**, 102–110 (2023).
22. Root, D. H., Melendez, R. I., Zaborszky, L. & Napier, T. C. The ventral pallidum: subregion-specific functional anatomy and roles in motivated behaviors. *Prog. Neurobiol.* **130**, 29–70 (2015).
23. Morais-Silva, G. & Lobo, M. K. Refining the circuits of drug addiction: the ventral pallidum. *Curr. Opin. Neurobiol.* **86**, 102883 (2024).
24. Li, Y. D. et al. Ventral pallidal GABAergic neurons control wakefulness associated with motivation through the ventral tegmental pathway. *Mol. Psychiatry* **26**, 2912–2928 (2020).
25. Luo, Y. J. et al. Ventral pallidal glutamatergic neurons regulate wakefulness and emotion through separated projections. *iScience* **26**, 107385 (2023).
26. Faget, L. et al. Opponent control of behavioral reinforcement by inhibitory and excitatory projections from the ventral pallidum. *Nat. Commun.* **9**, 849 (2018).
27. Tooley, J. et al. Glutamatergic ventral pallidal neurons modulate activity of the habenula-tegmental circuitry and constrain reward seeking. *Biol. Psychiatry* **83**, 1012–1023 (2018).
28. Liu, B., Cao, Y., Wang, J. & Dong, J. Excitatory transmission from ventral pallidum to lateral habenula mediates depression. *World J. Biol. Psychiatry* **21**, 627–633 (2020).
29. Prasad, A. A. & McNally, G. P. Ventral pallidum output pathways in context-induced reinstatement of alcohol seeking. *J. Neurosci.* **36**, 11716–11726 (2016).
30. Howells, F. M., Stein, D. J. & Russell, V. A. Synergistic tonic and phasic activity of the locus coeruleus norepinephrine (LC-NE) arousal system is required for optimal attentional performance. *Metab. Brain Dis.* **27**, 267–274 (2012).
31. Lelkes, Z., Porkka-Heiskanen, T. & Stenberg, D. Cholinergic basal forebrain structures are involved in the mediation of the arousal effect of noradre naline. *J. Sleep. Res.* **22**, 721–726 (2013).
32. Vazey, E. M. & Aston-Jones, G. Designer receptor manipulations reveal a role of the locus coeruleus noradrenergic system in isoflura ne general anesthesia. *Proc. Natl. Acad. Sci. USA* **111**, 3859–3864 (2014).
33. Beerling, W. et al. Physiological and hormonal responses to novelty exposure in rats are mainly related to ongoing behavi oral activity. *Physiol. Behav.* **103**, 412–420 (2011).
34. Harris, G. C. & Aston-Jones, G. Arousal and reward: a dichotomy in orexin function. *Trends Neurosci.* **29**, 571–577 (2006).
35. Richard, J. M., Ambroggi, F., Janak, P. H. & Fields, H. L. Ventral pallidum neurons encode incentive value and promote cue-elicited instrumental actions. *Neuron* **90**, 1165–1173 (2016).
36. Wang, F. et al. Salience processing by glutamatergic neurons in the ventral pallidum. *Sci. Bull.* **65**, 389–401 (2020).

37. Liu, D. et al. A common hub for sleep and motor control in the substantia nigra. *Science* **367**, 440–445 (2020).
38. Taylor, N. E. et al. Optogenetic activation of dopamine neurons in the ventral tegmental area induces reanimation from general anesthesia. *Proc. Natl. Acad. Sci. USA* **113**, 12826–12831 (2016).
39. Knowland, D. et al. Distinct ventral pallidal neural populations mediate separate symptoms of depression. *Cell* **170**, 284–297 e218 (2017).
40. Wulff, A. B., Tooley, J., Marconi, L. J. & Creed, M. C. Ventral pallidal modulation of aversion processing. *Brain Res.* **1713**, 62–69 (2019).
41. Yu, X. et al. GABA and glutamate neurons in the VTA regulate sleep and wakefulness. *Nat. Neurosci.* **22**, 106–119 (2019).
42. Gelegen, C. et al. Excitatory pathways from the lateral habenula enable propofol-induced sedation. *Curr. Biol.* **28**, 580–587 e585 (2018).
43. Carter, M. E., de Lecea, L. & Adamantidis, A. Functional wiring of hypocretin and LC-NE neurons: implications for arousal. *Front. Behav. Neurosci.* **7**, 43 (2013).
44. Hayat, H. et al. Locus coeruleus norepinephrine activity mediates sensory-evoked awakenings from sleep. *Sci. Adv.* **6**, eaaz4232 (2020).
45. Yamashita, T. & Yamanaka, A. Lateral hypothalamic circuits for sleep-wake control. *Curr. Opin. Neurobiol.* **44**, 94–100 (2017).
46. Stephenson-Jones, M. et al. Opposing contributions of GABAergic and glutamatergic ventral pallidal neurons to motivational behaviors. *Neuron* **105**, 921–933 (2020).
47. Liu, C. et al. Lateral habenula glutamatergic neurons modulate isoflurane anesthesia in mice. *Front. Mol. Neurosci.* **14**, 628996 (2021).
48. Yin, L. et al. Optogenetic/chemogenetic activation of GABAergic neurons in the ventral tegmental area facilitates general anesthesia via projections to the lateral hypothalamus in mice. *Front. Neural Circuits* **13**, 73 (2019).
49. Liang, Y. et al. The NAergic locus coeruleus-ventrolateral preoptic area neural circuit mediates rapid arousal from sleep. *Curr. Biol.* **31**, 3729–3742 (2021).
50. McCarren, H. S. et al. alpha2-Adrenergic stimulation of the ventrolateral preoptic nucleus destabilizes the anesthetic state. *J. Neurosci.* **34**, 16385–16396 (2014).
51. Ballesteros, J. J., Briscoe, J. B. & Ishizawa, Y. Neural signatures of α2-adrenergic agonist-induced unconsciousness and awakening by antagonist. *Elife* **9**, e57670 (2020).
52. Zhang, L. et al. Electroencephalogram mechanism of dexmedetomidine deepening sevoflurane anesthesia. *Front. Neurosci.* **16**, 913042 (2022).
53. Brown, R. E., Basheer, R., McKenna, J. T., Strecker, R. E. & McCarley, R. W. Control of sleep and wakefulness. *Physiol. Rev.* **92**, 1087–1187 (2012).
54. Wang, D. et al. Task-demand-dependent neural representation of odor information in the olfactory bulb and posterior piriform cortex. *J. Neurosci.* **39**, 10002–10018 (2019).
55. Wu, H. et al. Internal states influence the representation and modulation of food intake by subthalamic neurons. *Neurosci. Bull.* **36**, 1355–1368 (2020).
56. Ji, Y. W. et al. Differential remodeling of subthalamic projections to basal ganglia output nuclei and locomotor deficits in 6-OHDA-induced hemiparkinsonian mice. *Cell Rep.* **42**, 112178 (2023).
57. Jia, T. et al. A nigro-subthalamo-parabrachial pathway modulates pain-like behaviors. *Nat. Commun.* **13**, 7756 (2022).
58. Sun, H. et al. A common neuronal ensemble in nucleus accumbens regulates pain-like behaviour and sleep. *Nat. Commun.* **14**, 4700 (2023).
59. Luan, Y. et al. Reversal of hyperactive subthalamic circuits differentially mitigates pain hypersensitivity phenotypes in parkinsonian mice. *Proc. Natl. Acad. Sci. USA* **117**, 10045–10054 (2020).
60. Kelz, M. B. et al. An essential role for orexins in emergence from general anesthesia. *Proc. Natl. Acad. Sci. USA* **105**, 1309–1314 (2008).
61. Schneider, C. A., Rasband, W. S. & Eliceiri, K. W. NIH image to ImageJ: 25 years of image analysis. *Nat. Methods* **9**, 671–675 (2012).

Acknowledgements

This work was supported by the Sci-Tech Innovation 2030-Major Project (2021ZD0203100 (J.L.C.)), the National Natural Science Foundation of China (82271293 (C.X.), 82071231 (C.X.), 82171235 (C.Z.), 82371242 (C.Z.), 82471247 (C.X.)), the Fund for Jiangsu Province Specially-Appointed Professor (C.X. and C.Z.), the Natural Science Foundation of Jiangsu Province (BK20211349) (C.Z.), and the Leadership Program in Xuzhou Medical University (JBGS202203) (C.X.). X.Y.X., Y.X. and Y.J. acknowledge the Postgraduate Innovation Program in Jiangsu Province (KYCX23_ 2992, KYCX21_2714, and KYCX22_2935). We acknowledge Terrence Xiao for data organization and English grammar check.

Author contributions

C.X., C.Z. and J.L.C. designed and supervised this research. X.Y.X. and C.X. collected, analyzed, and illustrated the electrophysiological data. X.Y.X., Y.X., X.L., Y.H., Y.J. and Y.W.J. performed the mouse survival surgeries and morphological experiments. X.Y.X., Y.X., X.L. and Y.H. performed the EEG recordings and behavioral tests. X.Y.X., Y.X., Y.H. and Y.G. managed the mouse colony. X.Y.X., C.X. and Y.X. collected the imaging data. C.X., X.Y.X., C.Z., J.L.C., S.L. and J.J.Y. organized data and wrote the manuscript. All authors read and approved the manuscript.

Competing interests

The authors declare no competing interests.

Additional information

Supplementary information The online version contains supplementary material available at https://doi.org/10.1038/s41467-025-59857-1.

Correspondence and requests for materials should be addressed to Jun-Li Cao, Chunyi Zhou or Cheng Xiao.

Peer review information *Nature Communications* thanks Ji Hu, and the other anonymous reviewer(s) for their contribution to the peer review of this work. A peer review file is available.